Cover Page

Federal Agency and Organization Element to Which Report is Submitted	Department of Energy Office of Energy Efficiency and Renewable Energy
Federal Grant or Other Identifying Number Assigned by Agency	DE-EE0009199
Project Title	Final Report: Ducted Fuel Injection And Cooled Spray Technologies For Particulate Control In Heavy-duty Diesel Engines
PD/PI Name, Title and Contact Information (e-mail address and phone number)	PI Contact Information: Adam Klingbeil, PhD Engineering Technical Leader (518)-693-2944 Adam.Klingbeil@Wabtec.com
Name of Submitting Official, Title, and Contact Information (e-mail address and phone number), if other than PD/PI	
Submission Date	06/30/2024
Recipient Organization (Name and Address)	Westinghouse Air Brake Technologies Corporation 30 Isabella St. Pittsburgh, PA 15212-5862
Project/Grant Period (Start Date, End Date)	10/01/2020-02/28/2024
Reporting Period End Date	03/31/2024
Report Term or Frequency (annual, semi-annual, quarterly, final, other)	final

Acknowledgment: This material is based upon work supported by the U.S. Department of Energy's Office of Energy Efficiency and Renewable Energy (EERE) under the Vehicle Technologies Office (VTO) Award Number DE-EE0009199.

1. Executive Summary

Cooled Spray (CS) and Ducted Fuel Injection (DFI) are in-cylinder technologies for diesel engines that can reduce particulate matter and soot emissions and data has been published showing that these technologies can reduce soot emissions by 75-100% for some engines at some operating conditions. However, little is known about scaling the devices for engine size. Additionally, the performance of either technology over the engine duty cycle has not been explored. This project addresses both of these points through single-cylinder engine investigations.

The objectives of this project are to provide details about dimensional scaling of these devices and to demonstrate 75% PM reduction over a range of operating conditions on a single-cylinder engine. Two engines were used for this project: a 125mm bore optically accessible engine at Sandia National Laboratories and a 168mm bore metal engine at Southwest Research Institute. The optical engine was used to study the performance of DFI and CS inserts for a large injector orifice diameter injector that is characteristic of a locomotive engine and to perform scaling studies for DFI. The metal engine was used to perform scaling and alignment studies for CS and to evaluate the technology for both EGR and non-EGR engines over the engine operating map.

Modifications were required for both engines to accept the prototype inserts being tested. The optical engine required a new fuel injector, cylinder head and piston so that tests could be run at the pressures and engine speeds required. Additionally, a novel rotating stage was designed for the optical engine to simplify alignment of the modules. The metal engine required a modified cylinder head to accept CS inserts and a modified piston to provide additional space around the fuel injector for the CS inserts.

Tests on the optical engine showed that DFI reduces PM emissions for both small injector orifices (0.170mm diameter) and large injector orifices (0.290mm). For high load testing, the DFI modules were not as effective as at low load testing, but it was acknowledged that minimal geometric optimization was performed and more improvements may be possible. Comparing DFI to CS and conventional diesel combustion (CDC), DFI performed better than CS or CDC. The CS geometries used in these studies may not be ideal for that engine and additional modifications likely would improve performance.

Tests on the metal engine showed PM reductions as high has 80% at some operating conditions with duty-cycle PM reductions of ~50% for EGR and non-EGR configurations. The CS testing on the metal engine showed that chamfering of the fuel passage inlet either through hydro-erosion or mechanical grinding provided significant improvements in the PM reduction capabilities of the insert. Additionally, alignment sensitivities were explored and the data show that the tolerance to misalignment is approximately 0.05 to 0.1mm for the inserts that were studied here. Air-fuel ratio was shown to be important in the effectiveness of the CS inserts. In several tests, it was shown that the CS inserts are more effective at reducing the PM for high-AFR operating conditions compared to low AFR conditions.

In summary, multiple designs were evaluated on both engines. It was found that for the conditions and configurations studied here, a fuel passage diameter of ~2.5mm performed best overall. Significant duty-cycle PM reductions are possible using these technologies and sensitivities to AFR, alignment fuel passage diameter and inlet fuel passage shaping were

explored and are reported here. More PM reduction may be possible with improved geometric design and attention to alignment practices.

2. Introduction

The purpose of this project is to evaluate the performance of ducted fuel injection (DFI) and cooled spray (CS) technologies in heavy-duty diesel engines with the objective of significantly expanding the knowledge base around these technologies and to demonstrate the potential of these technologies for reducing PM emissions in real engines. DFI and CS are in-cylinder technologies for diesel engines that can be used to modify the combustion event to reduce or eliminate soot and PM formation in the combustion chamber.

However, only limited testing has been done with these technologies and it is important to determine if these technologies will be effective over the entire engine operating map and furthermore, it is not yet understood how the design parameters of these technologies should scale with different sized engines. To address those two needs, this project has two primary goals:

1) Provide critical dimensional scaling guidance for DFI and CS technologies
2) Demonstrate more than 75% PM reduction over a range of operating conditions using CS technology

The project was executed primarily through engine testing at two facilities. An optical engine at Sandia National Laboratories was used to perform imaging investigations and to compare DFI and CS technologies. Additionally, significant prior work has been published exploring DFI in the Sandia engine. The project described herein was directed toward larger engines such as those used in locomotives. Wabtec has a single-cylinder engine installed at Southwest Research Institute and most of the CS investigations were performed on that engine. The setup at SwRI allowed for broader performance sweeps and more frequent change of insert geometries. Together, the test facilities provided significant learnings that will help further the development of DFI and CS technologies.

3. Experimental Setup

This project was primarily based on experimental testing in two single-cylinder engines (SCE's). An optically accessible single-cylinder research engine at Sandia National Laboratories was used to investigate the effects of ducted fuel injection (DFI) and Cooled Spray (CS) on the combustion and mixing behavior for conditions resembling those of a locomotive engine. The second engine was a single-cylinder high-speed engine that is installed at Southwest Research Institute (SwRI). The engine design is based on Wabtec's high-speed engine platform, but it is a single-cylinder engine with independent control of the engine boundary conditions to enable flexible exploration of new engine technologies. Both engines required modifications for this project and the details of the modifications are provided in this section.

In addition to engine modifications, alignment techniques were required for aligning the DFI and CS hardware to the fuel injectors. Two different techniques are described here and the benefits and challenges of each are discussed. Lastly, the DFI and CS devices needed to be manufactured. Different manufacturing and finishing strategies for the devices were evaluated over the course of this project and are described below.

1. Characteristics of the setup

Two SCE's were used in this study. Key parameters for the two engines are provided in Table 1. The Sandia engine has a smaller bore and stroke and operates at a lower compression ratio than the Wabtec engine. However, experiments were defined to provide similar conditions for the two engines. In this project, the optical engine focused on performing fundamental scaling studies for DFI and CS while the metal engine focused on meeting the target 75% PM reduction over the duty cycle.

Table 1: Engine geometry properties

		Sandia Optical Engine	Wabtec Engine
Bore	mm	125	168
Stroke	mm	140	198
Compression Ratio		12.5	16
Displacement	L	1.72	4.4
Rated Speed	RPM	1800	1800
Rated Power	kW/Cyl	~52	155
Fuel System		Common Rail	Common Rail

For SCE testing, it is important to define the boundary conditions so that the in-cylinder conditions are consistent with what would be seen in a production engine. Additionally, the range of operating conditions needs to be defined. Since the metal engine represents the platform of interest, all conditions were set based on that engine and the optical engine was adjusted to match the metal engine. As a starting point, we determined the speed and load of the metal engine for the supplemental engine test (SET)[1], which is shown in Figure 1. The size of the data points represents the weighting factor used for each condition when calculating duty cycle performance. The numbers next to each data point indicate the mode number of each condition. The y-axis is based on the rated torque of the engine.

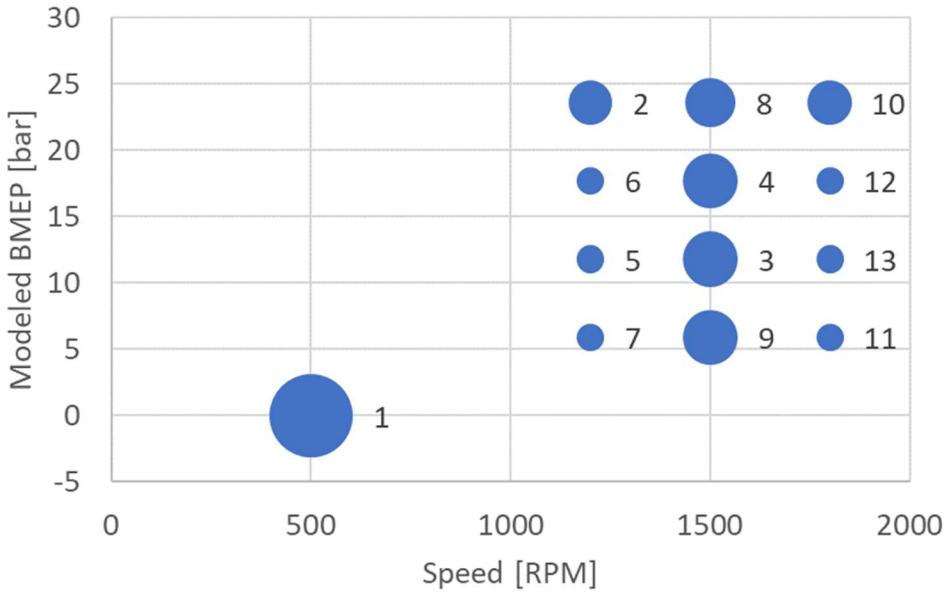

Figure 1: Speed, load and weighting factors for the duty cycle considered in this study.

Once the engine set points were determined, the boundary conditions for the single-cylinder engine (SCE's) were needed. An SCE typically is not turbocharged like a typical multi-cylinder engine (MCE). Rather, the experimental arrangement simulates turbocharging with compressed air and a back-pressure valve. Ideally, the boundary conditions for the SCE are set so that the individual cylinder of the engine behaves as if it were one cylinder of an MCE. Hence, the boundary conditions are selected to try to match the in-cylinder conditions between the SCE and the MCE during the combustion event. To facilitate this matching, a GT-Power model of the engine was developed using a simple turbo with variable turbine mass flow multiplier. The variable turbine mass flow multiplier was used to simulate a variable geometry turbocharger, which would provide the needed air-handling flexibility over the range of speed and load considered for this duty cycle. This model allowed us to evaluate realistic operating conditions over the engine map so that appropriate SCE boundary conditions could be determined.

After defining the operating conditions of the metal SCE, it was also necessary to define the boundary conditions for the optical engine. While the optical SCE has different geometry, it is possible to match in-cylinder thermodynamic conditions, and that is what was done here. The intake temperature and pressure were adjusted so that the unburned charge near TDC of compression was similar to that of the metal SCE. Additionally, for some conditions the oxygen content of the charge gas was adjusted by adding nitrogen to the intake air to simulate the effects of exhaust gas recirculation in the metal SCE for the same operating mode.

In addition to the matching of thermodynamic conditions near TDC and charge gas mixture oxygen content, additional constraints were used for the fuel injection system to provide a combustion system that was similar between the two engines. For the metal SCE, an injector was selected based on previous experience with this engine. For the optical engine, it was desired to create a combustion plume that closely resembled that of the metal engine. To achieve this, the injector hole size was matched between the two engines along with the fuel injection quantity per hole. However, since the optical engine has a smaller displacement and can trap less air, a 2-hole injector was used rather than the 6-hole injector used in the metal engine. Thus, in this manner,

the thermodynamic conditions and the individual combustion plumes were matched between the two engines.

2. Modifications to the setup

Both SCE's required modifications to the arrangement in order to perform the tasks required for this project. The optical engine required a new piston and cylinder head to meet the speed and pressure requirements for this project. Additionally, an updated fuel injection system and data acquisition system were required. The metal engine required modifications to the cylinder head to accept CS components and a new piston was procured to provide sufficient space near the injector without impacting the piston. Details of the modifications are provided below.

1. Optical Engine Redesign

The conditions required for the optical engine for this study were more demanding than what has been required of that engine in the past and an updated cylinder head and piston were required to withstand those conditions. The updates also provided the opportunity to make some additional improvements to facilitate DFI alignment and to accept an updated fuel injector. The data acquisition system was updated for this project because the previous system could not sample fast enough for the tests performed at the higher engine speeds planned in this program.

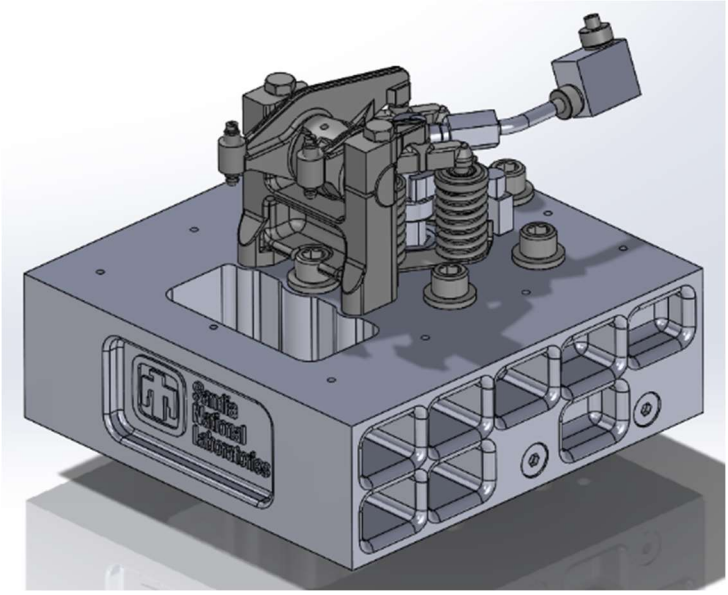

Figure 2: 3D model of the redesigned cylinder head for the optical engine.

The cylinder head for the optical engine was redesigned to be rated for 200bar operation (see Figure 2). This is higher than what was tested in the past on this engine and represents a significant capability upgrade. In addition, the head was equipped with a rotating stage for mounting DFI hardware (See Figure 3). Past tests on this engine with DFI required a significant amount of time adjusting the DFI modules to be aligned with the fuel injector. An iterative process of installing the insert, checking alignment and then adjusting with rotation and shims had been used to align the components. By designing a rotating stage into the head, one degree

of alignment (rotation between injector and DFI module) could be adjusted on the fly, thereby simplifying and expediting the alignment process.

In Figure 3, the different pieces of the rotating stage are visible. The injector sleeve is threaded into the fixed portion of the stage. The DFI module is bolted to a gear, that allows it to be rotated with high precision to adjust the rotational alignment. A clamp is then used to clamp the assembly in place after the DFI module has been properly aligned.

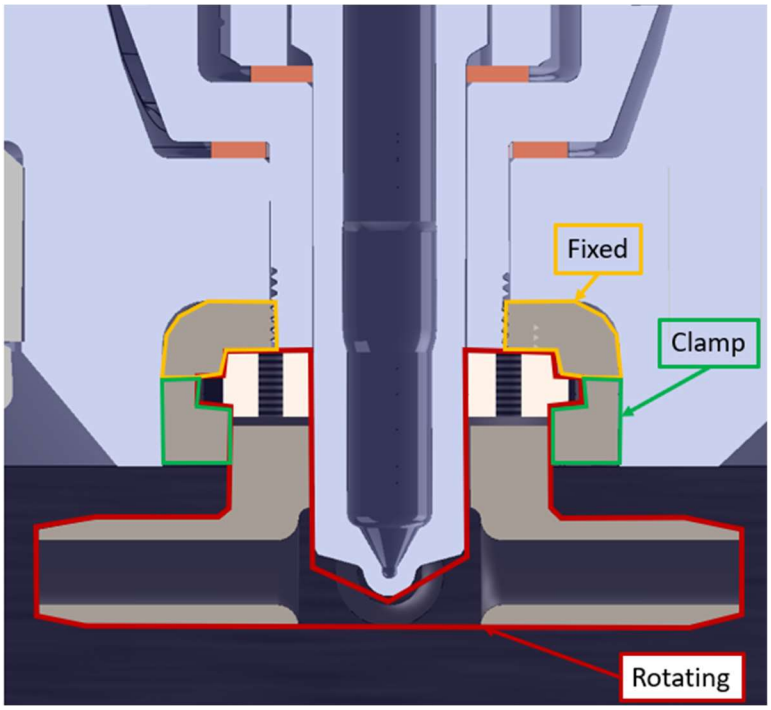

Figure 3: Cross section view of the redesigned cylinder head showing the key features of the rotating stage.

The cylinder pressures and engine speeds planned for this study also required a new optical piston design. The combination of higher speeds and higher cylinder pressures meant that the piston needed to be simultaneously strong and light. The crown was also modified to increase the field of view through the piston from the high speed imaging system. A model of the piston and crown are shown in Figure 4.

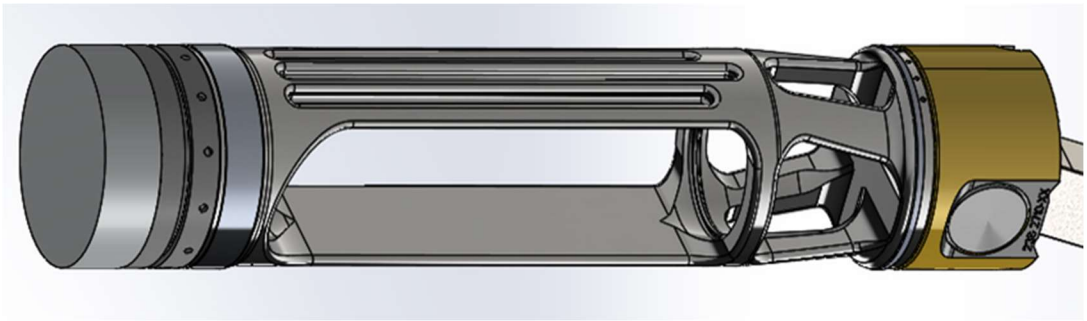

Figure 4: Piston and piston crown for the optical engine used in this project.

The redesigned piston crown required significant efforts and the first design was not successful. The first crown design utilized a stepped sapphire window that was brazed into a

Kovar window holder. Kovar was selected because it has thermal expansion properties similar to those of sapphire. Sapphire was selected for the window because of its strength and optical transparency in the wavelength ranges of interest. After the window was brazed into the holder, the window cracked in several places and was not capable of sealing against pressure. Attempts were made to salvage the original design, but eventually a new piston crown design was selected that simplified the geometry of the window and allowed epoxy to be used to seal the crown. This design, shown in Figure 5 was successful throughout the testing that was performed for this project and utilized a simpler, less expensive window design. An all-metal piston-top assembly was also designed, which was used in early tests to evaluate the engine performance while the optical piston was being built. That piston is also shown in Figure 5

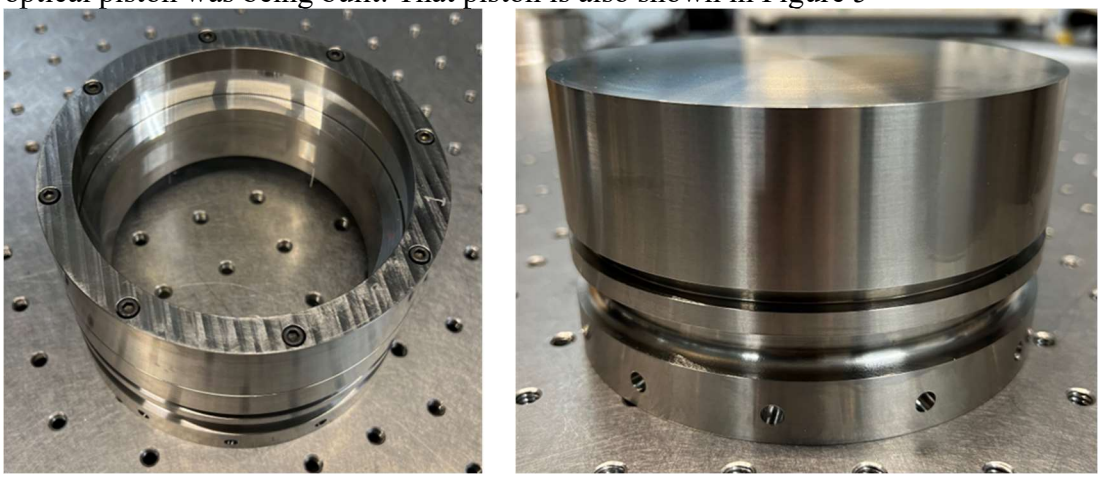

Figure 5: Redesigned optical piston crown (left) and metal piston crown (right) designed for the optical engine.

Finally, new fuel injectors were required to better match the characteristics of the injectors used in the locomotive engine. New injectors were procured and the nozzle tips were modified by Exergy Engineering. Off-the-shelf injectors were purchased by the vendor and the original nozzle holes were welded shut and new holes were drilled in the nozzles to meet our specifications. An image of one of the injector tips is shown in Figure 6.

Figure 6: Image of fuel injector used in optical engine

2. Metal Engine Head Design

The metal engine required some modifications as well in order to accept the CS inserts used for this project. The region around the fuel injector nozzle was bored to a larger diameter to allow a CS insert to be installed, as shown in Figure 7. The insert was installed and held in place by the threaded end of the injector sleeve. This arrangement allowed the insert to be secured in

place, but also enabled the rotational alignment to be adjusted to line up with the injector through a series of iterative alignment steps. Note there is a modified region in the cylinder head that was bored out to create space for the CS insert. This is a clearance fit at room temperature but because of thermal expansion of the materials, it is an interference fit when the engine is operating.

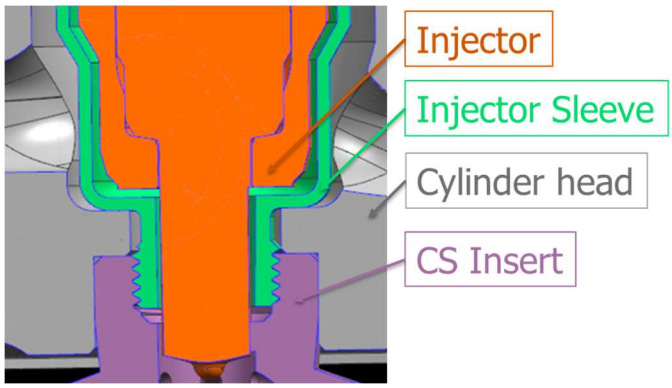

Figure 7: Mounting arrangement for CS inserts inside the metal engine.

Recognizing that the CS inserts would absorb heat, it was important in the design to provide good thermal contact between the insert and the cylinder head so that the insert could be properly cooled. However, the cylinder head and insert are different materials with different coefficients of thermal expansion, so it was also important to control the dimensions of the bore and the insert seating diameter. If the insert expanded too much inside the cylinder head, there would be risk of mechanical damage possibly leading to cracking of the cylinder head.

A thermal analysis was performed on the insert and cylinder head. Heat transfer coefficients to the insert were based on previous simulations for in-cylinder components. The result of the analysis is shown in Figure 8 where the outer edges of the insert are very hot but the base of the insert that is mounted in the cylinder head is a similar temperature to the cylinder head in that same region.

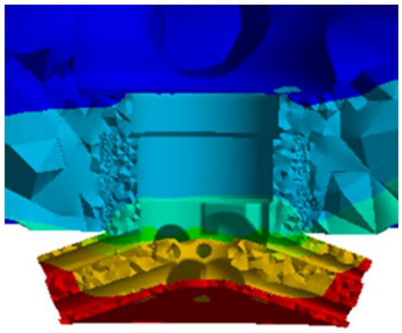

Figure 8: Steady state thermal profile predicted for full load operation.

Once the temperature profile was available, an FEA was performed on the cylinder head to evaluate the stress caused by mechanical deformation at high cylinder pressure in combination with the stresses caused by thermal distortion of the head and insert. Of particular concern was the region in the cylinder head where the insert contacts the cylinder head. When the combustion gases heat the insert, it expands and creates stress in the cylinder head where the insert contacts

the head. It was necessary to evaluate the cylinder head stresses to ensure that the thermal stresses in this region don't exceed structural limitations.

Results of the stress analysis of the cylinder head bore are shown in Figure 9 where the largest stresses are observed near the combustion side of the bore. The highest temperatures of the insert are on the combustion side and as one probes the temperatures of the insert deeper inside the cylinder head, the temperatures are lower. Because of this, the largest stress is in the region where the insert has contact with the cylinder head but is closer to the high temperatures.

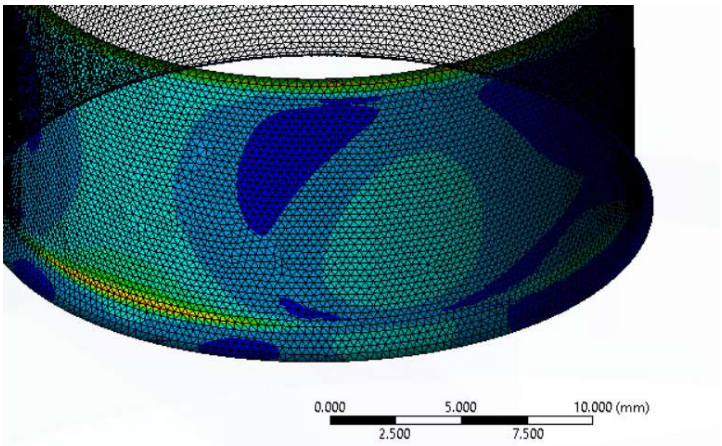

Figure 9: Stress analysis of the cylinder head under expected operating conditions.

The design of the cylinder head and the insert mounting region was adjusted so that all calculated stresses were within design guidelines and therefore the risk of mechanical failure was low. The final design modifications were implemented on two cylinder heads and multiple inserts were generated in this project that could be swapped in and out of the heads. Figure 10 shows a picture of the modified cylinder head and one CS insert that was used under this project.

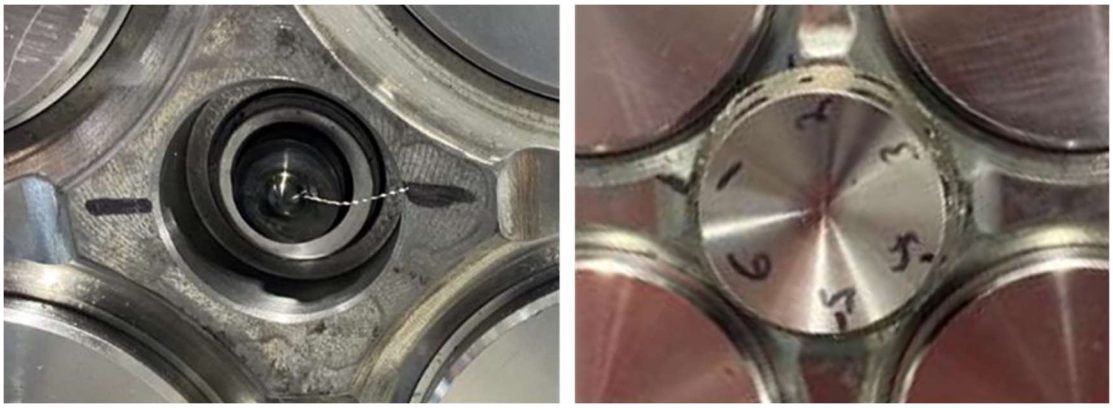

Figure 10: Modified cylinder head to accept CS insert (left) and CS insert installed in the cylinder head (right).

Another design change that was required under this project was a modification to the injector washer. With the modifications to the cylinder head, it was found that the stresses in the injector sleeve were increased and there was concern about failure of the injector sleeve after torquing the injector in place. To remedy this, a new crush washer was designed to move the injector clamping load away from the center of the injector, thereby reducing the shear stress in the injector sleeve. The original and redesigned washers are shown in Figure 11.

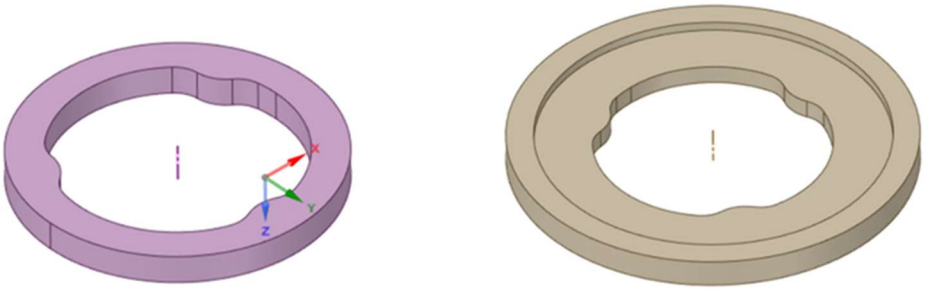

Figure 11: Original injector washer (left) and new injector washer (right).

Finally, the metal engine required a modified piston for this project. The production piston has a center pip that is very close to the fuel injector and would not allow sufficient space near the injector for many of the designs that were being considered for this project. Thus a new piston was design that had a similar shape and identical compression ratio, but provided more space near the fuel injector. Figure 12 shows the original and redesigned bowl geometries.

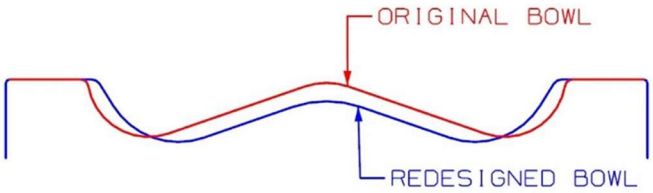

Figure 12: Outline of the original piston bowl and the redesigned piston bowl.

3. Alignment Techniques

Alignment between the fuel injector holes and the DFI or CS fuel passages is an important factor. If the components are poorly aligned then the fuel will impinge on the inserts, rather than passing through the fuel passages into the main combustion chamber. It was also important in this project to characterize the sensitivity of the inserts to misalignment. Because of this, it was necessary to have an alignment measurement technique that could be used to characterize the misalignment between the fuel injector hole and the fuel passage. Two alignment measurement techniques were evaluated in this project. The first technique used a fiber optic borescope inserted into the fuel passage to image the fuel injector hole within the fuel passage of the DFI or CS insert. The second technique involved inserting a silicone plug into the fuel passage, injecting fuel, and observing the witness marks of the fuel spray on the plug to characterize the misalignment between the fuel passage and the injector spray hole. More details about the alignment techniques are provided below.

1. Fiber Optic (Sandia and SwRI)

The fiber optic alignment method used a fiber optic borescope inserted into the fuel passages to image the fuel injector holes from inside the fuel passages. The borescope was flexible, but the

imaging portion of the borescope had a rigid section approximately 100mm in length. Additionally, custom sleeves were made for the imaging section so the outer diameter of the rigid section could be increased to fit snugly within the fuel passage of the insert. The imaging section of the borescope is shown in Figure 13. The sleeve was marked to control the orientation and insertion depth of the borescope so that images were recorded consistently from measurement to measurement.

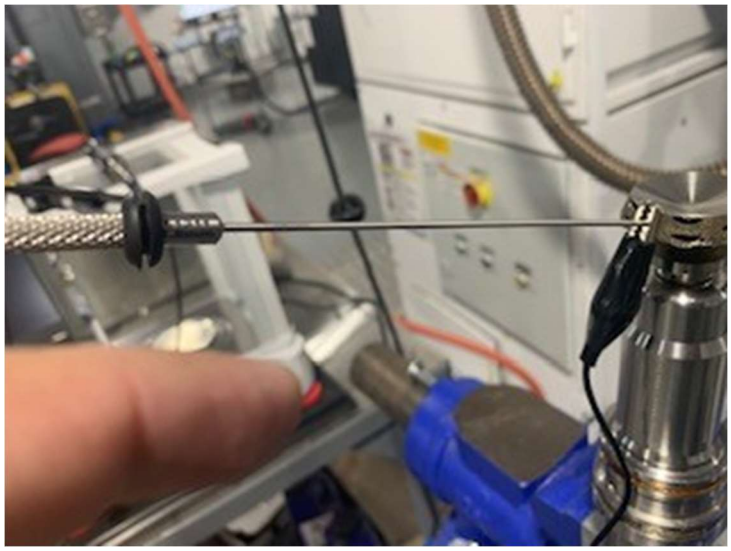

Figure 13: Borescope imaging section with sleeve.

Sample images from the borescope are shown in Figure 14. The insertion depth of the borescope was controlled so that a portion of the inside opening of the fuel passage was visible and the fuel injector hole was also visible. The images were then processed to measure the distance between the center of the fuel passage opening and the center of the injector orifice. The measured distance was scaled relative to the fuel passage opening in order to determine the quantitative offset between the fuel passage and the injector orifice.

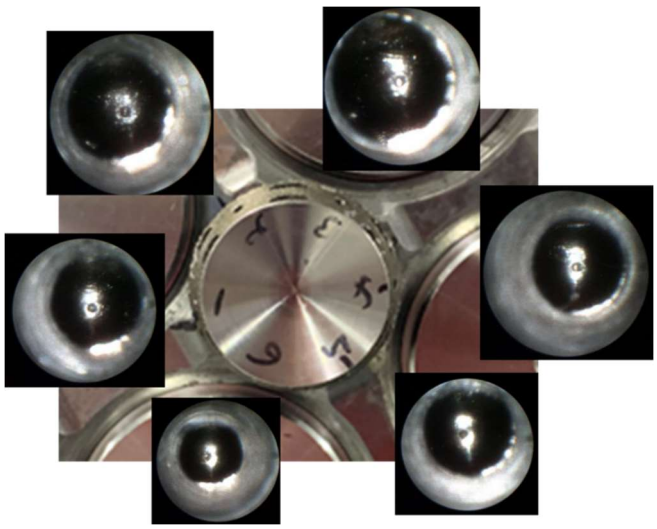

Figure 14: Borescope images of the fuel injector holes taken from the fuel passages for a fixed alignment.

Several sources of measurement bias were noted in this method. First, it is possible that the fuel injector orifice is centered in the fuel passage, but if the spray angle is not aligned, then the fuel injector spray may still be off target. Second, it was observed that the borescope lens is not perfectly centered on the end of the borescope. This can lead to an error in the offset measurement between the fuel injector orifice and the fuel passage. Hence, these sources of error can lead to a measurement bias error in determining the offset between the fuel injector orifice and the fuel passage. To overcome this, multiple alignments were tested with many of the inserts to determine which alignment offset provided the best overall performance.

2. Spray plug (Sandia and SwRI)

The second alignment measurement technique is the so-called ‘spray plug method’. In this method, a silicon plug was inserted into the fuel passages of the CS or DFI insert and the fuel injector was injected for several shots. The impact of the high-pressure fuel spray is sufficient to leave a mark on the plug. A photo of the plug could then be used to measure the location of the impact mark relative to the outer edge of the plug.

A sample image of one of the spray plugs is shown in Figure 15. The top of the spray plug was marked in black to determine the rotational alignment of the plug after it was removed from the fuel passage. The small circle at the center of the image indicates the center of the impact mark from the fuel spray. The location of this mark relative to the center of the plug was calculated and used to quantify the offset of the insert.

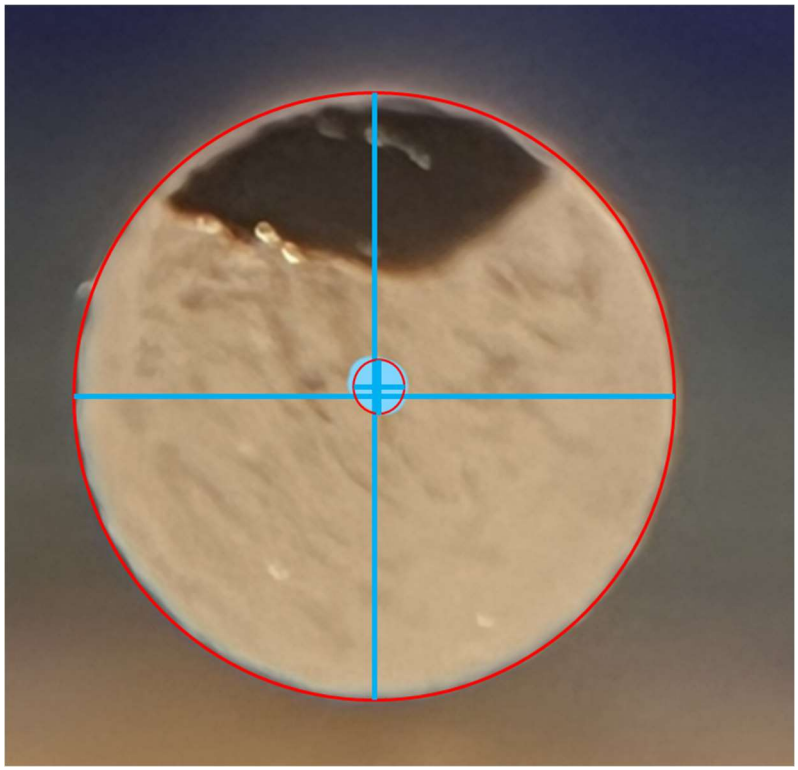

Figure 15: Image of spray plug used to determine alignment of a CS insert.

Both measurement methods were evaluated on both the metal and optical engines. Most of the tests on the optical engine used an open DFI insert where the spray plugs could easily be

inserted into the fuel passage and an injection pulse could be commanded. Additionally, test time on the optical engine was limited due to the nature of the test facility. For these reasons, the spray plug method was preferred over the optical method. The spray plug method on that engine was straightforward to perform and the limited test time made testing of multiple alignments undesirable.

On the metal engine, CS inserts were primarily tested and once installed on the cylinder head, access to the inlet of the fuel passage was not possible, so the spray plugs were inserted from the outside, which presented some additional challenges. Furthermore, commanding a fuel injection even required that the engine be warmed up and motored prior to injecting and this added significant effort to the spray plug method. However, the optical alignment technique was straightforward and therefore the metal engine relied most often on the optical alignment technique with some limited verifications of the alignment using the spray plug method.

4. Manufacturing techniques

The CS inserts designed for this project had varying degrees of complexity and required manufacturing techniques that were flexible with small geometries, but also precise at small scales. Additive manufacturing was used to generate the CS inserts and after printing, the inserts were finish-machined in regions where more precise dimensions were required. Images of the as-printed and as-finished insert are shown in Figure 16. Additive manufacturing was useful for quickly prototyping new designs to be tested, but the technique is not precise enough for the critical surfaces and additional machining was required. The inserts were printed from Inconel 718 because it maintains strength at high temperatures and is commonly used in metal additive manufacturing.

Figure 16: Images of a CS insert after printing (left) and after finish machining (right).

For this project, it was critical that the fuel passages be manufactured accurately. Initially, the fuel passages were drilled using a 5-axis machining arrangement. While the material used for the inserts created some challenges, it was found that the fuel passages could be drilled. One additional step that was performed with some of the drilled inserts was chamfering of the fuel passage inlets. In some DFI tests, it was found that chamfering of the DFI duct inlet improved overall performance. Chamfering of some of the drilled fuel passages was performed on some of the CS inserts and it will be shown that this showed varying amounts of improvement depending on the insert and the operating condition, but it was mostly successful in improving PM emissions compared to non-chamfered inserts.

A second technique was also evaluated whereby the fuel passages were printed. Typically, printing the fuel passages would leave a coarse surface on the inside of the fuel passages, particularly on the overhanging sections of the fuel passage. To address this issue, some were manufactured with printed fuel passages, but then an additional post-processing step known as hydro-erosion or hydro-grinding was used to polish the fuel passages to a smooth finish. This allowed the fuel passages to be printed in a very precise location, but the hydro-erosion process removes material, so the fuel passages were printed with artificially small-diameter fuel passages and the hydro-erosion subsequently removed the roughness and the excess material.

The hydro-erosion step presents two additional disadvantages that are not present with the drilling process. First, the inserts required custom fixturing and a specialty vendor to perform the work, leading to an increase of several weeks lead time for completing the inserts. Second, it was found that the hydro-erosion process removes more material near the inlet and outlet of the fuel passages, leading to an hourglass-shaped fuel passage, rather than a straight cylinder. This could be compensated for through iterative design by changing the as-printed diameter as a function of position within the fuel passage, but that was beyond the scope of this work.

Figure 17 shows an image of the fixture used to perform hydro-erosion on a CS insert. The abrasive slurry was fed through the top of the insert and the air passages were blocked off so the slurry would only pass through the fuel passages. Different geometries required different fixtures in order to block the air passages and ensure that the abrasive fluid passed through the fuel passages as intended.

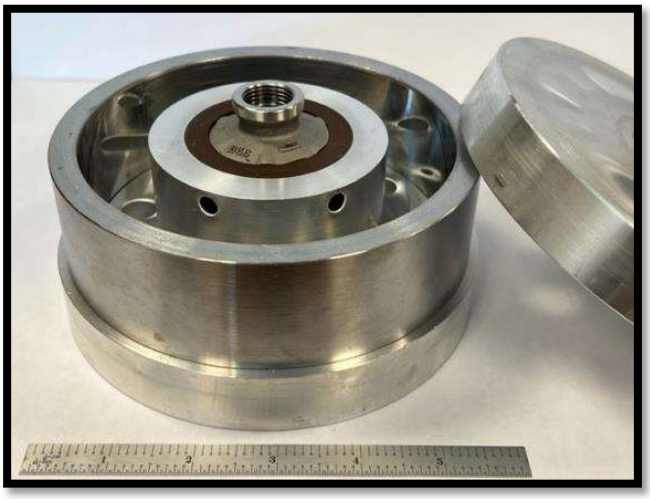

Figure 17: Image of a CS insert mounted inside a fixture used in the hydro-erosion process.

Figure 18 shows images of the inlet of two fuel passages in an insert before and after hydro-erosion. The improvement in surface finish is clear from these images. Before hydro-erosion, the fuel passage is rough and has metal particles hanging down into the opening. After hydro-erosion, the surface is smooth and the metal particles have been removed.

Figure 18: Images of two fuel passage inlets before and after hydro-erosion.

4. Optical Engine Testing

1. Operating conditions for Optical Engine

This project aimed to operate similar conditions between the optically accessible engine at Sandia and the metal engine at SwRI. However, the bore, stroke, compression ratio and displacement volume are all different between these two engines. The approach selected was to match the combustion plumes between the two engines. To do this, the fuel injector hole size was matched between the optical and metal engines, but the number of holes was not. Additionally, the thermodynamic conditions at TDC and the oxygen content of the charge gas mixture were matched, so the fuel would be injected into charge gas with the same characteristics. It was recognized that the piston geometries are different and the smaller bore size of the optical engine may present some additional interference in the optical engine that wasn't present in the metal engine, so some differences in performance are expected.

Two operating conditions were selected for operation on the optical engine. The two conditions were Mode 4 with and without EGR. These conditions were selected because they pushed the optical engine to a higher speed and load than previously tested and they fall near the center of the SET operating map. With conditions selected, the intake boost pressure of the optical engine was adjusted so that the pressure at TDC would match the metal SCE. Additionally, the MAT of the optical engine was selected so that the calculated temperature at TDC would match between the two engines. Because of its lower compression ratio, the optical engine required a higher MAT and MAP to reach the same TDC conditions. The final conditions for the optical SCE are listed in Table 2.

Table 2: Summary of condition set points for running the optical engine at a Mode 4 condition that matches the Wabtec metal SCE.

Parameter	EGR Condition	Non-EGR Condition
Injector-tip configuration	2 × .288 mm × 155°	
Injected fuel quantity	144.2 mg/stroke	152.2 mg/stroke
Injection pressure (P_{inj})	220 MPa	150 MPa
Injector-tip protrusion	4.5 mm	
Engine speed	1500 RPM	
Intake-O_2 mole fraction (XO_2)	17.0 mol%	20.95 mol%
Start of combustion (SOC)	Swept	
Intake manifold abs. press. (IMAP)	4.00 bar	3.50 bar
Motored cylinder pressure at TDC	133 bar	123 bar
Intake manifold temperature (IMT)	83 °C	71 °C
Motored bulk in-cylinder temperature at TDC	890 K	860 K
Fuel	Off-road No. 2 diesel	

Multiple DFI and CS inserts were tested on the optical engine and compared to the baseline engine performance without an insert. The key geometric features of the DFI and CS inserts that were tested in the optical engine are listed in Table 3. The DFI geometries were selected based on prior DFI experience and data published in open literature. The CS geometries were selected based on CS testing on the metal engine at SwRI and based on the DFI results from the optical engine.

Table 3: Summary of DFI and CS geometry tested on the optical engine.

Identifier	Config	Fuel Passage Diameter	Fuel Passage Length	Standoff Distance
		[mm]	[mm]	[mm]
2D2.5L12G3δ	DFI	2.5	12	3.0
2D3.0L12G3δ	DFI	3.0	12	3.0
2D3.5L12G3δ	DFI	3.5	12	3.0
562925P21	CS	3.0	12	2.5
562925P22	CS	2.5	12	2.5

2. Testing to high load

Initial tests were performed in the upgraded Sandia optically accessible SCE with four-hole injector tips[2]. These tests were not meant to mimic conditions on the Wabtec SCE, but only to evaluate DFI in the engine after the new cylinder head, piston, and fuel injector were installed. For these conditions and this hardware, the soot reduction using DFI was 40-60%, however, NOx emissions also increased. These results represent the highest BMEP and torque that this

engine has ever produced. It was noted that the reduction in soot emissions was not as dramatic as has been observed in previous studies on this engine. There are several possible reasons including spray/duct misalignment. However, one that stands out is that the nozzle geometry is different with a higher flow and the nozzle holes angled higher up towards the top of the piston. Tests with a smaller flow nozzle showed even worse performance so it is likely that the nozzle hole angle is contributing to this difference.

It was also observed that the injection rate profile for the injectors used in this project is different than the rate profile used in previous studies. A sample injection rate profile is shown in Figure 19. In previous studies on this engine, the rise of the injection profile was much faster, but in this injection profile, the rise from start of injection to full injection rate requires almost 1 msec (7.2 crank-angle degrees at 1200 RPM). This difference in injection rate profile may also have an impact on the effectiveness of DFI, but further evaluation of the injection rate profile was not within the scope of this project. The observed shape of the injection profile for this injector is consistent with the injection profiles observed for the Wabtec highspeed engine. While DFI did not reduce the PM emissions as much as in previous experiments at Sandia, the initial studies of DFI on this engine did show reasonable soot reduction over a broad range of BMEP levels.

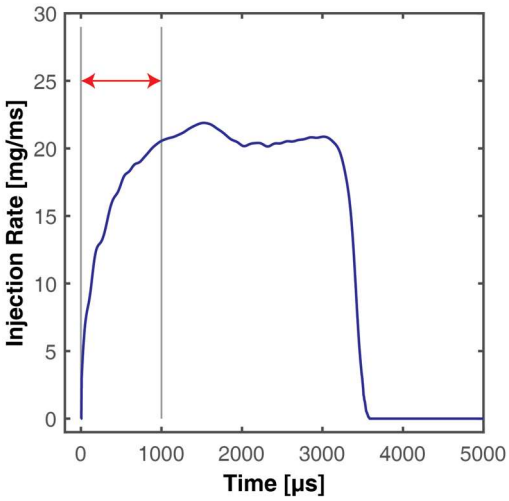

Figure 19: Sample injection rate profile for the injector tested on the Sandia optical engine.

3. EGR and non-EGR results

Summary performance data from the optical engine for Mode 4 non-EGR operation are shown in Figure 20. The conventional diesel combustion (CDC) data represent the baseline operation without a DFI or CS insert. The start of combustion was varied from -5 to +7 deg to characterize how the engine performance changes over this range. A CS insert and a DFI insert are compared in the plot, each with a 2.5mm diameter fuel passage. It was found that the inserts with the 2.5mm fuel passages performed best for this engine at this condition, so the plots included here summarize the best results for DFI and CS compared to CDC.

There are some interesting details to note about the data shown here, particularly regarding the sensitivity to injection timing. Over this range of injection timings, the NOx emissions do not

significantly change for CDC, DFI or CS. Typically, one would expect that as the timing is advanced to an earlier start of combustion, the NOx emissions would increase, but in this case, that sensitivity is not observed. Another unexpected observation is that as the start of combustion is advanced, the PM emissions increase. In a typical diesel engine, it is often observed that earlier start of combustion leads to higher NOx and lower PM emissions so this behavior is again unexpected. The combustion efficiency for all three configurations improves with later injection timings, but the overall thermodynamic efficiency decreases with later timings. Even though combustion efficiency is improving with later timings, the later combustion event results in less efficient extraction of the energy and lower overall efficiency.

Comparing DFI to CDC, the soot emissions have decreased by 50-60%, but the NOx emissions have increased 10-25%. While the ignition delay is longer for DFI than CDC, the duration of combustion is shorter and the overall thermodynamic efficiency is improved at all operating conditions, but particularly at late combustion timings.

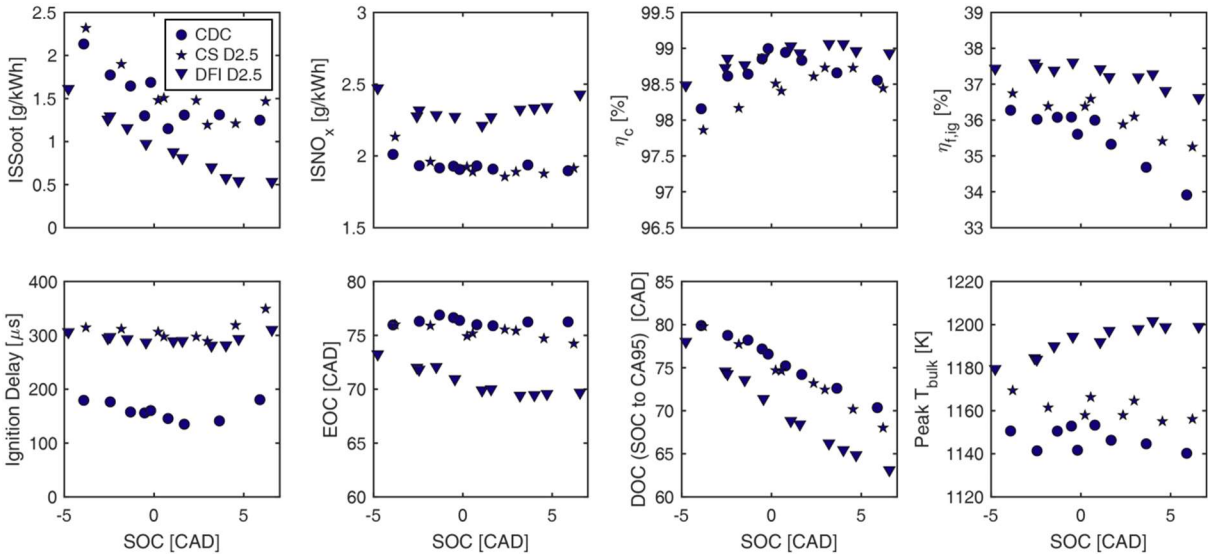

Figure 20: Optical engine test results of CDC, DFI and CS configurations operating at Mode 4 without EGR.

Comparing CDC to CS for non-EGR operation, the NOx emissions are the same and the soot emissions are also similar. While the combustion efficiency for CS is worse than that of CDC, the overall thermodynamic efficiency for CS is slightly better than that of CDC. Because only a minor change in performance was observed, it is likely that this CS design may not be optimal for this engine configuration.

Mode 4 operation was also evaluated with EGR for the same hardware configurations and summary results are plotted in Figure 21. In this case, the trends with start of combustion again are similar for CDC, DFI and CS. As start of combustion is advanced, the soot emissions again increase. However, as start of combustion is advanced, the NOx emissions also increase. So in this case, later timings result in improved NOx and soot emissions. For later combustion timings, the CDC overall efficiency quickly drops off while the DFI and CS efficiencies are somewhat steady over the range tested but the highest efficiency points are at later start of combustion timings. Hence, the DFI and CS inserts can operate with late combustion timings and simultaneously improve efficiency as well as NOx and soot emissions.

Comparing CDC to DFI in the EGR cases, the soot has improved with DFI. This is particularly true at late combustion timings where the largest relative improvement in soot

emissions is observed. At these late timings, the combustion efficiency as well as the overall thermodynamic efficiency has improved for DFI while for CDC, the combustion efficiency has improved but overall thermodynamic efficiency is degraded.

The performance of CS falls somewhere between that of CDC and DFI. The soot emissions are reduced and the overall efficiency is improved for CS compared to CDC, but not as much as DFI. The NOx emissions for CDC and CS match closely except at the earliest timings. For late timings, the NOx emissions of CDC and CS match closely while the DFI case shows an increase. Overall, both CS and DFI are showing improved combustion compared to the CDC case.

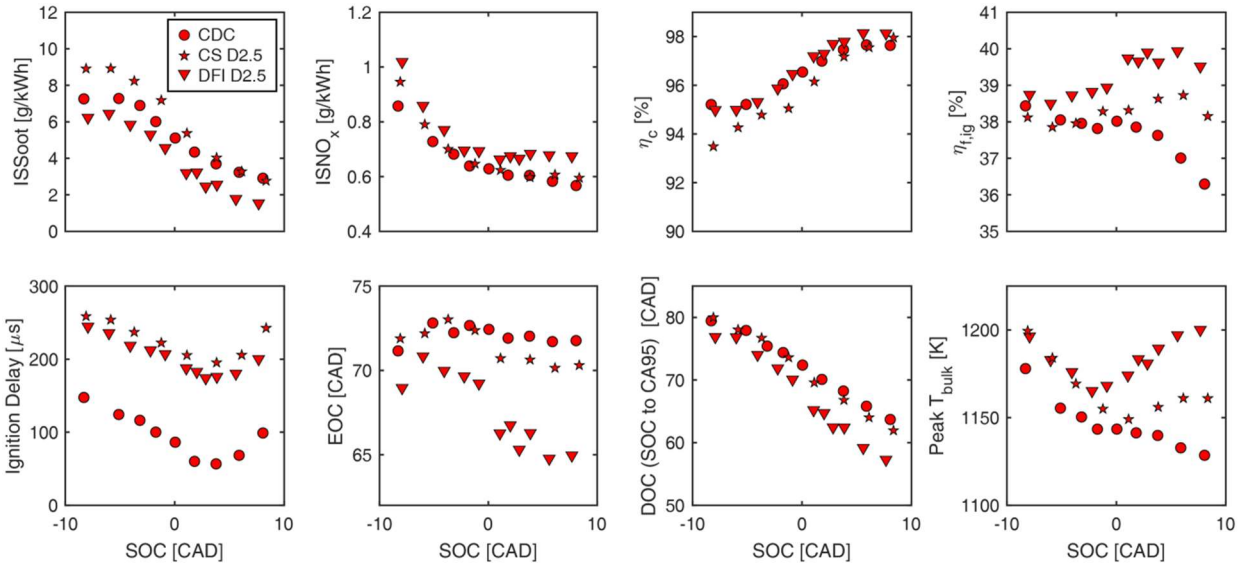

Figure 21: Optical engine test results of CDC, DFI and CS configurations operating at Mode 4 with EGR.

4. Cost function and performance at optimal cost function

With the large amount of conventional diesel combustion (CDC), cooled spray (CS), and ducted fuel injection (DFI) experimental data acquired in this project, a cost function was created to compare the performance of CDC, CS, and DFI objectively across operating conditions. This helped to facilitate quantitative comparisons among the techniques in terms of efficiency and emissions.

One challenge that arises when comparing different combustion strategies across different operating conditions (e.g., CDC, CS, and DFI both with and without EGR in the present project) is how to rank the overall performance of each strategy quantitatively. For example, one strategy may have higher soot emissions but lower NO_x and efficiency than another making it challenging to determine which configuration resulted in the best overall performance. A cost function, C_i, was created to allow comparison of operating conditions when several critical performance parameters were different for each operating condition:

$$C_i \equiv \frac{ISEC_i - min(ISEC)}{max(ISEC) - min(ISEC)} + \frac{ISNO_{x,i} - min(ISNO_x)}{min(ISNO_x)} + \frac{ISSoot_i - min(ISSoot)}{min(ISSoot)} \quad (1)$$

where i is an index that is unique to a given combustion strategy and operating condition; $ISEC$ stands for indicated specific energy consumption and is defined as the reciprocal of the

gross indicated fuel-conversion efficiency; $ISNO_x$ and $ISSoot$ are the indicated-specific NO_x and soot emissions, respectively; and the minimum and maximum values for each parameter are obtained using the results from all combustion strategies and all operating conditions from the dataset at the same simulated-EGR level. As seen from Eq. 1, the cost function is always ≥ 0, the best performance is achieved when the cost function is minimized, and the cost function is sensitive to small changes in $ISEC$ because its term is normalized by the range of $ISEC$ values in the dataset rather than simply the minimum value.

Using the cost function as defined in Eq. 1, it was determined that the best CS and DFI performance was obtained with a duct diameter of 2.5 mm for both the EGR and non-EGR conditions. The cost-function results for the non-EGR condition are shown in Figure 22, which indicates that the best performance for all techniques is achieved by DFI at a start-of-combustion (SOC) timing of 4.0 CAD ATDC. At their optimal timings, the largest contributors to the cost functions for CDC and CS are $ISSoot$ and $ISEC$, whereas the largest contributor to the cost function for DFI is $ISNO_x$.

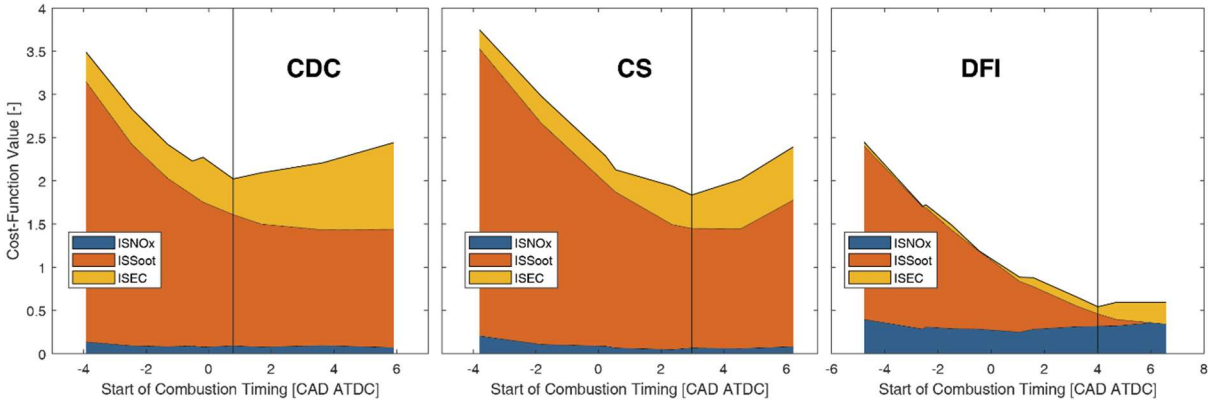

Figure 22: Total cost-function values and contributions from its three terms as functions of SOC timing for CDC (left), CS (middle), and DFI (right) at Mode 4 without simulated EGR (21 mol% oxygen in the intake mixture). The duct diameter used for DFI and the fuel passage diameter for CS results was 2.5 mm.

The cost-function results for the EGR condition are shown in Figure 23, which indicates that the best performance for all techniques is achieved by DFI at a retarded start-of-combustion (SOC) timing of 5.6 CAD ATDC (crank-angle degrees after top-dead-center). At their optimal timings, the largest contributors to the cost functions for CDC and CS are $ISSoot$ followed by $ISEC$, whereas the largest contributor to the cost function for DFI is $ISNO_x$.

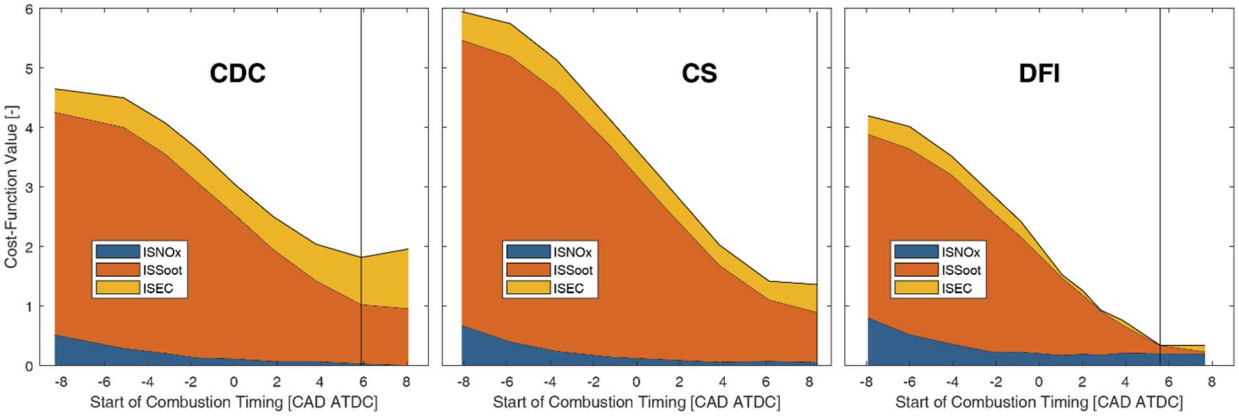

Figure 23: Total cost-function values and contributions from its three terms as functions of start-of-combustion (SOC) timing for CDC (left), CS (middle), and DFI (right) at Mode 4 with simulated EGR (17 mol% oxygen in the intake mixture). The duct diameter used for DFI and the fuel passage diameter for CS results was 2.5 mm.

Table 4 shows the optimal SOC timings and the corresponding cost-function values for the three combustion strategies at the two EGR levels. It is evident that both CS and DFI can provide benefits relative to CDC, with DFI providing the greatest performance improvements at the selected test conditions.

Table 4: Optimal SOC timings and cost-function values for CDC, CS, and DFI at Mode 4 with and without simulated EGR. The duct diameter used for DFI and the fuel passage diameter for CS results was 2.5 mm.

Operating Condition		Optimal SOC [CAD]	Optimal Cost-Function Value [-]
EGR	CDC	5.9	1.82
	CS	8.4	1.36
	DFI	5.6	0.34
Non-EGR	CDC	0.8	2.02
	CS	3.0	1.84
	DFI	4.0	0.54

5. Optical engine image analysis

The timeseries and imaging data from the optical engine are being analyzed with the goal of improving understanding of the mechanisms responsible for the performance differences across combustion strategies and operating conditions. This is an involved process, because it includes spatially aligning, temporally synchronizing, overlaying, displaying, and analyzing data from multiple input sources for each combustion strategy and operating condition. The images show high-speed natural luminosity (NL) and OH* chemiluminescence (CL) images with CS or DFI outlines overlayed, flame liftoff length (LoL) overlayed on the CL images, and timeseries data showing apparent heat-release rate (AHRR), spatially integrated natural luminosity (SINL), and fuel-injection rate.

An example frame from a movie for CDC, CS, and DFI operation at the EGR condition at the SOC that provided the minimum cost-function value is shown in Figure 24-Figure 26 respectively. It is interesting to note that the CDC and DFI cases had a minimum cost function at a similar SOC while the CS arrangement had a minimum cost function at a later start of combustion.

Each frame is at CA30, the crank angle at which 30% of the heat-release has occurred. The image on the left is NL, and the image in the center is CL. The white dot at the center of each image is the injector tip, the white circle indicates the position of the piston bowl-rim, and the yellow markers on the CL image show the instantaneous LoL. The number in the upper-left corner of each image is the crank angle at which it was acquired, whereas the number in the lower-left corner is the time since the actual start of fuel injection. All displayed images were acquired on the second fired cycle of a collection of seven fired cycles that were imaged for each combustion strategy and operating condition. Piston-window fouling from soot typically becomes evident by the fifth fired cycle for these conditions.

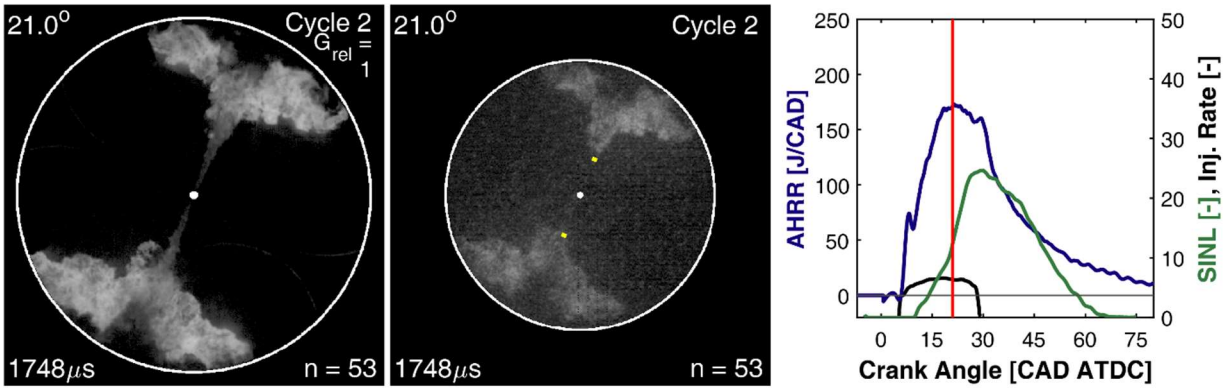

Figure 24: Image of CDC at CA30 for the EGR condition with SOC = 5.9 CAD ATDC, which yielded the minimum CDC cost-function value.

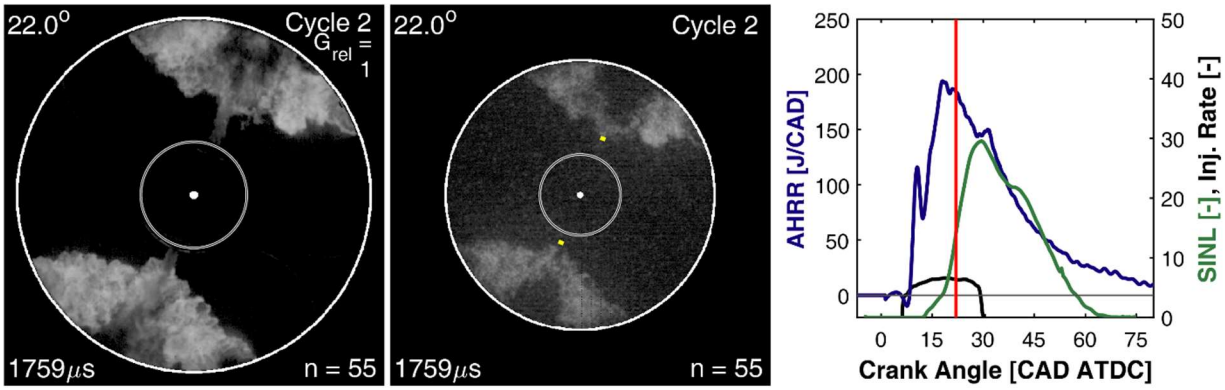

Figure 25: Image of CS combustion at CA30 for the EGR condition with SOC = 8.4 CAD ATDC, which yielded the minimum CS cost-function value. The fuel-passage diameter and length were 2.5 and 12 mm, respectively.

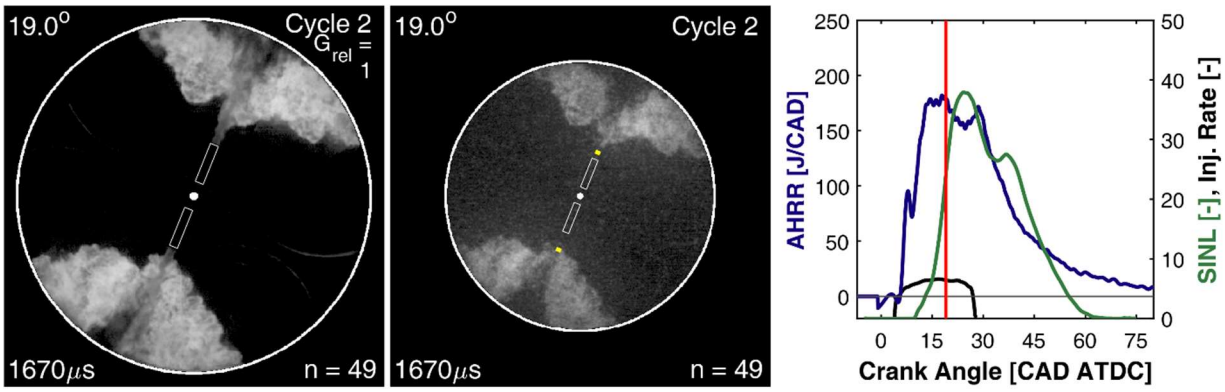

Figure 26: Image of DFI combustion at CA30 for the EGR condition with SOC = 5.6 CAD ATDC, which yielded the minimum DFI cost-function value. The duct diameter and length were 2.5 and 12 mm, respectively.

Comparing these three conditions, it should be noted that the CDC condition has the highest engine out soot emissions, followed by the CS condition and the DFI condition has significantly lower soot emissions than the other two. In the CDC image, a dark region near the outer rim of the bowl suggests that a large amount of soot is being produced in that region. For the DFI condition with the lowest engine-out soot among the three data sets, the darkened region is smaller and less intense, consistent with more luminosity and higher temperatures.

The performance data from the testing on the optical engine showed that soot emissions were much higher for early injection timings than for late injection timings. Images for an early and a late injection timing condition for CDC, CS and DFI are shown in Figure 27-Figure 29. In each case, the pair of images on the left represents the early start of combustion and the pair of images on the right represents the late start of combustion. In the CDC images, it is clear that the LoL has increased for the later timing and this is expected. For the CS and DFI cases, no impact on LoL is observable and it is likely that the flame is at the fuel passage exit or inside the fuel passage in both cases.

One trend is consistent for all three sets of images. In each set of images, the early injection timing case shows a triangle-shaped darkened region in the center of the plume near the outer bore of the piston. For the later start of combustion timings, this darkened region is reduced in size and moved more towards the outer rim. It is possible that for the early timings, the piston is higher in the cylinder and interfering more with the combustion plume. The plume would normally be reacting and emitting luminescence around the perimeter, but in this region, where the plume is pressed against the piston, the reactions are quenched. This may be partially responsible for the increased soot at early start of combustion, but there may be other phenomena that are even more impactful to the performance and a conclusion cannot be drawn from these images. At the time of this writing, data analysis of the optical engine data is ongoing and preparation of a publication describing detailed results is underway.

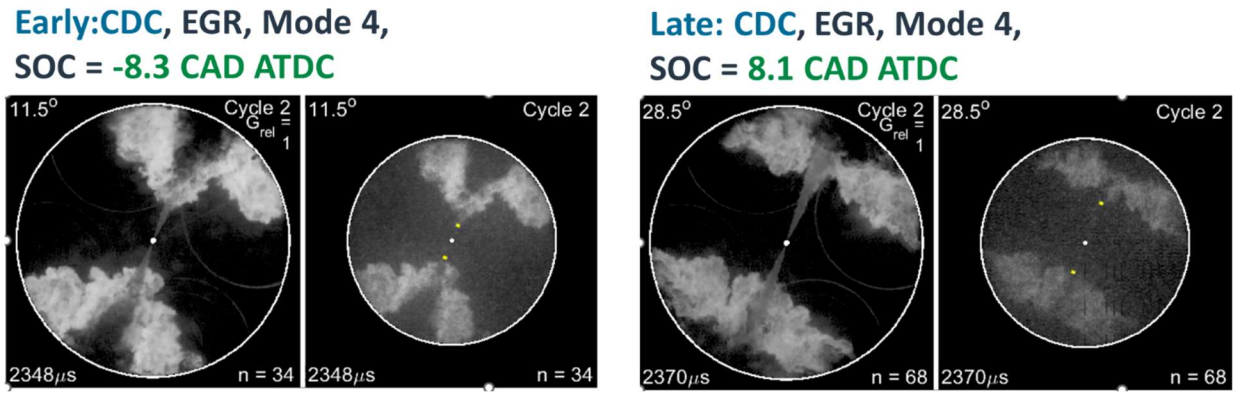

Figure 27: Images for CDC combustion near the end of the combustion event.

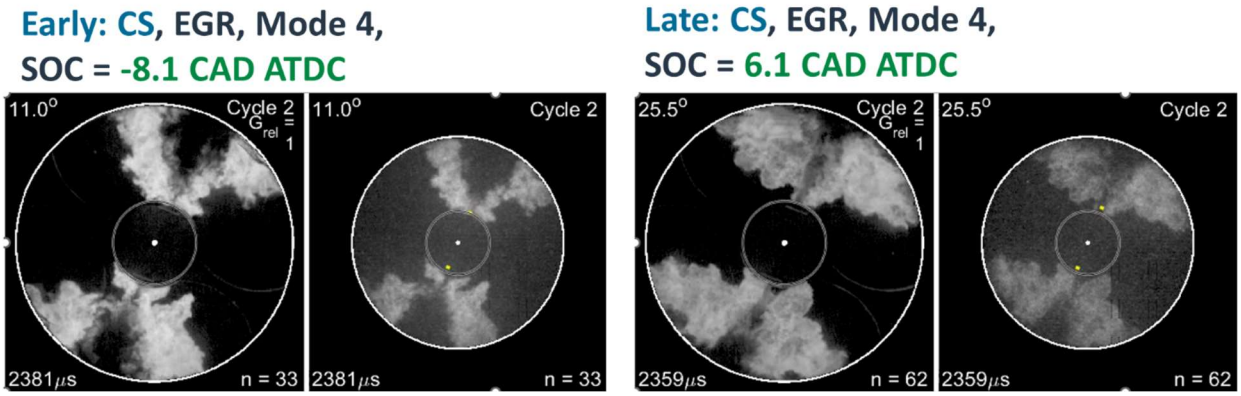

Figure 28: Images for CS combustion near the end of the combustion event.

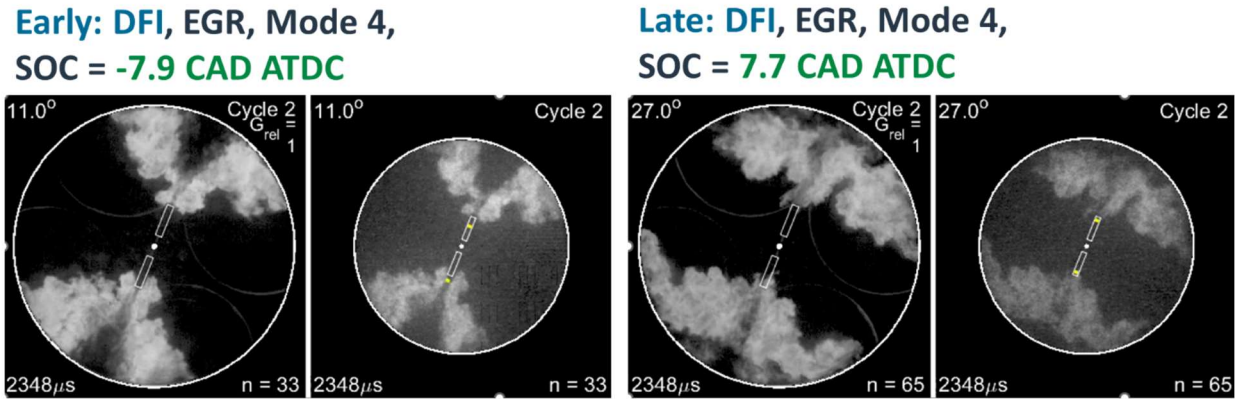

Figure 29: Images for CS combustion near the end of the combustion event.

5. Metal Engine Testing

1. Operating Conditions: SET and weighting factors, EGR and non-EGR, Boundary condition selection

The metal SCE was operated over a range of speed and load conditions defined by the 13-mode supplemental engine tests (SET). Both an EGR and a non-EGR engine were considered for this project. The SCE doesn't use a normal turbocharger, but instead, intake pressure and temperature as well as exhaust pressure can all be independently varied. Therefore, 1D engine

modeling was required to determine appropriate boundary conditions for each of the operating modes. A variable geometry turbocharger was simulated for this engine with different size characteristics for the non-EGR and EGR version of the engine. Based on prior experience, the EGR version of the engine was operated at higher boost levels than the non-EGR version, but the AFR of the non-EGR version was higher.

While the 1D modeling provided an initial set of operating conditions for the engine, in some cases parameters were varied that would normally drive a response in the turbocharger. The 1D simulations were not repeated for all operating conditions when changes were made. In the case of injection timing and rail pressure adjustments, no changes were made to the boundary conditions. In cases where the AFR was varied by increasing or decreasing the boost pressure, the engine exhaust pressure was incremented or decremented by the same amount to maintain a fixed pressure difference across the engine. Thus, the non-CS baseline condition is the operating condition for the conventional diesel combustion case where no other changes have been made to any boundary conditions except the injection timing has been adjusted for constant NOx emissions. For all conditions evaluated here between the CS and non-CS baseline, the same boundary conditions were used when comparing the two. If CS was evaluated at an increased boost pressure, then the non-CS baseline was evaluated at the same increased boost pressure and the two data sets were compared.

2. Compare SCE to MCE

When the engine was commissioned, initial testing was performed to compare the emissions from the SCE to those from the MCE. Several operating conditions were selected from low to high power and emissions data were recorded. Figure 30 shows a comparison between the SCE and MCE for these conditions. The NOx and CO emissions agree well between the two engines. The PM emissions are higher on the SCE, but the relative trends are similar for the two engines.

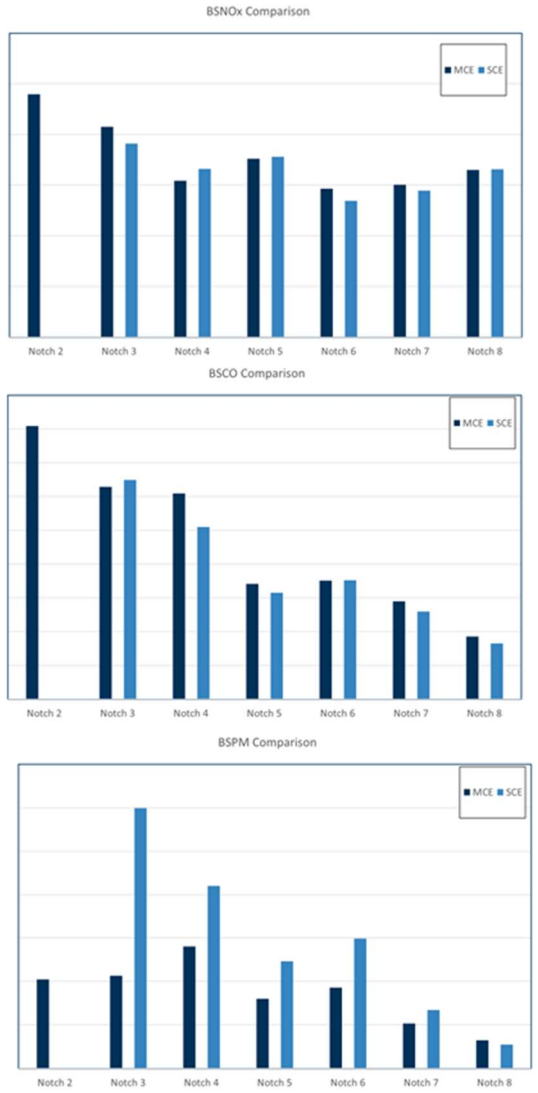

Figure 30: Comparison of NOx, CO and PM between the SCE and an MCE at locomotive operating conditions.

3. Insert Testing

Numerous CS inserts were tested on the metal SCE over the course of this project and many of the inserts that were tested were evaluated with multiple alignments. This section of the report will review key results from the testing, but is not meant to show all results of every test.

The first inserts tested in this project were printed inserts with drilled fuel passages. Two geometries were generated that were nearly identical with the exception of the fuel passage diameter. One of the geometries had a 2.0mm diameter fuel passage and the other had a 1.0mm diameter fuel passage. These two inserts were tested with a higher flow nozzle (injector orifice diameter ~0.32mm) at Mode 5 conditions.

Normalized FSN is plotted in Figure 31 for these two inserts compared to the non-CS baseline. For the CS tests, injection timing was adjusted to match the NOx of the baseline condition at the baseline injection timing. By operating at constant NOx emissions, a more direct comparison of performance impact of CS is provided. For this insert design at this operating

condition, the 1mm diameter fuel passage shows a ~4.5x increase in FSN at the same NOx emissions while the 2mm diameter insert increased FSN by approximately 2.2x. Thus, both CS variants are showing an increase in FSN emissions compared to the baseline non-CS conditions, suggesting that some features of the insert design are resulting in detrimental performance. These results also suggest that a larger fuel passage diameter may be preferable compared to a smaller diameter. It is possible that the 1mm diameter fuel passage is too small for accurate alignment between the insert and the injector and the 2mm diameter fuel passages may be more tolerant to misalignment.

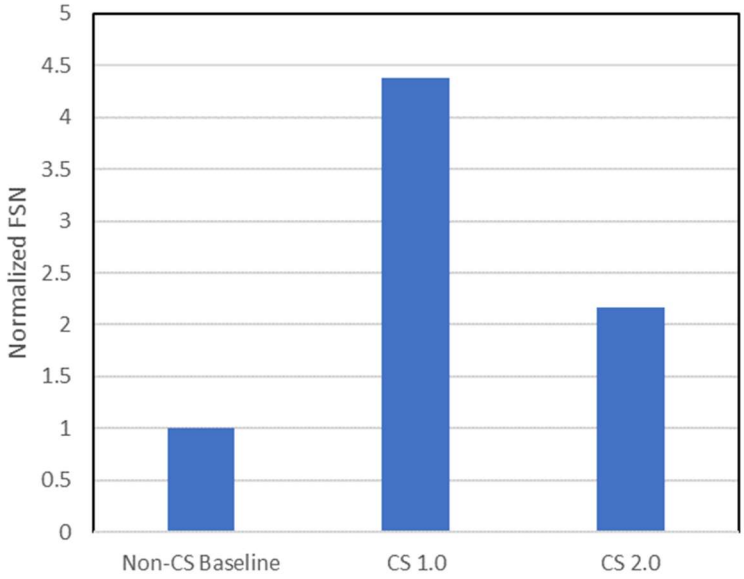

Figure 31: Normalized FSN for 3 hardware configurations at Mode 5 non-EGR conditions at constant NOx emissions. The injector nozzle for these tests had fuel injector orifices of 0.32mm nominal diameter.

The 2mm diameter insert was also tested with a lower flow nozzle (~0.29mm injector orifice diameter) at multiple conditions including Modes 2, 8 and 10 which are all 100% torque conditions but at speeds of 1200, 1500 and 1800RPM respectively. The FSN reduction of the insert is plotted in Figure 32 for these three operating conditions all tested with the same CS alignment. An interesting trend is observed in the results. For the lowest engine speed condition, Mode 2, the CS insert shows a ~65% reduction in FSN compared to the baseline condition at the same NOx emissions. For Mode 8 operation, at the intermediate speed of 1500RPM, no difference is observed and at 1800 RPM, a 40% increase in FSN is observed with the CS insert compared to the baseline. Thus, for this combination of insert and nozzle geometry, an improvement is seen at the low engine speed, 100% load condition, but performance degradation is observed at the highest speed 100% load condition. At most other operating conditions, the performance with the CS insert was not better than the baseline condition. This data illustrates that a performance change at some operating conditions with CS technology may be offset by performance changes at other operating conditions and it is critical to evaluate the CS technology over the expected operating range to properly characterize its impact on performance. Additional details regarding the performance of these inserts can be found in [1].

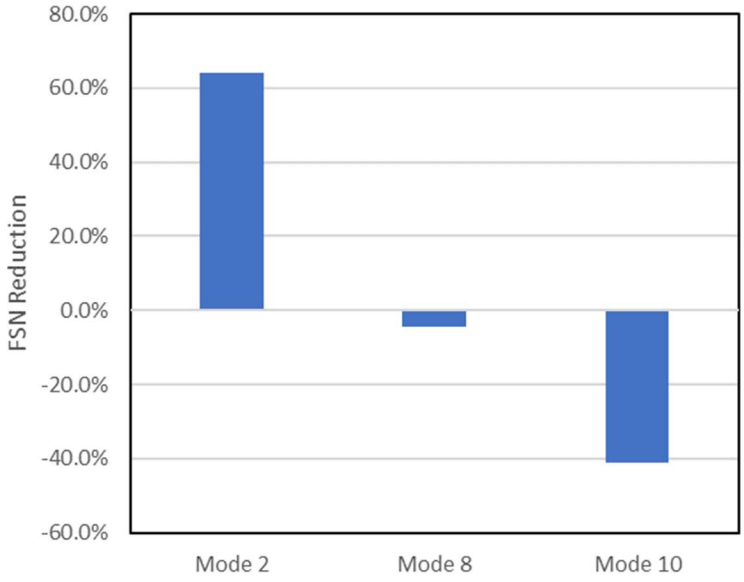

Figure 32: FSN Reduction at non-EGR conditions using the CS insert with 2.0mm fuel passage diameter for three different full-torque operating conditions at constant NOx.The injector nozzle for these tests had fuel injector orifices of 0.29mm nominal diameter. The CS insert alignment was not changed between operating conditions.

1. First hydro-eroded inserts

An alternative manufacturing process that was explored in this project was to print the fuel passages of the CS inserts rather than drilling them. Due to the nature of the additive manufacturing process, the surface finish of the fuel passages was rough and an additional post-processing step was required to remove the roughness. A process known as abrasive flow machining or hydro-erosion was used to improve the surface finish of the fuel passages. In hydro-erosion, an abrasive slurry is pushed through the fuel passages to wear down the rough surfaces and make them smooth.

Figure 33 compares the NOx and FSN for the non-CS baseline, a CS insert with 2.0mm diameter fuel passages and a CS insert with ~2.5mm printed and hydro-eroded fuel passages. The data show clear improvements in soot emissions compared to the baseline condition. The fuel passage diameter is slightly larger than the previously tested inserts (~2.5mm vs 2.0 mm for the drilled insert) but the results suggest that the hydro-erosion process is significantly improving the performance of the insert. Note that for the printed and hydro-eroded insert, the fuel passages were printed cylindrical but after hydro-erosion, the fuel passage shape was more hourglass shaped with a narrower section in the middle (~2.5mm diameter) and a wider section at the entrance and exit (~2.8-3.5mm). A more detailed description of the performance with this insert can be found in [4].

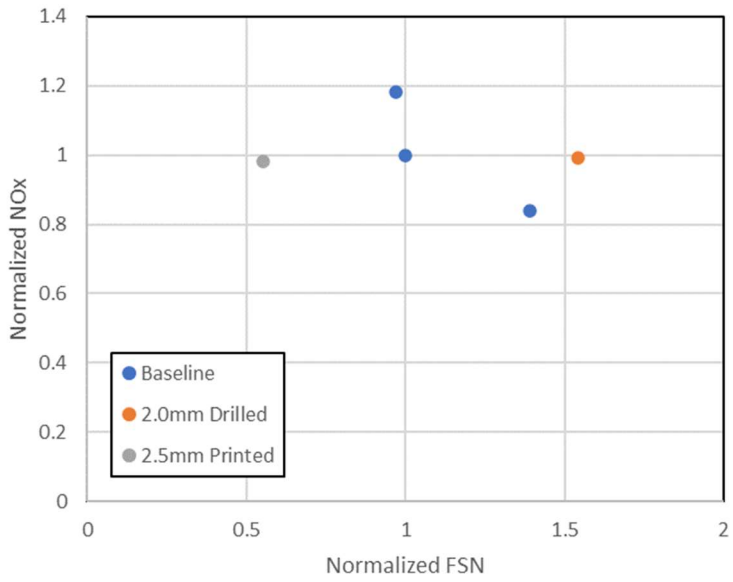

Figure 33: NOx versus FSN for Mode 5 non-EGR operation comparing the non-CS baseline to inserts with drilled fuel passages and printed/hydro-eroded fuel passages with injector orifice diameter of 0.29mm.

2. Temp-plug testing

At the beginning of the project, an analysis was performed to estimate the temperature profile throughout the volume of a CS insert and from that an FEA was performed to evaluate stress and thermal expansion. The project team designed a custom insert with threaded holes to accept Temp plugs so that the temperature profile could be validated or improved. A temp plug is a special screw with a material of known properties at the tip of the screw. The screws can be installed on a component and put into an environment of unknown conditions for some time. By subjecting the component to steady conditions of interest for sufficient time, the hardness of the material will change. That hardness can be measured and, knowing the amount of time at the condition of interest, the nominal temperature can be calculated.

The insert had positions for 9 temp plugs, but one of the threaded holes was damaged and not capable of accepting a temp plug. Of the remaining 8 holes, 4 were placed near the top of the insert where the insert would fit into the cylinder head and 4 were placed near the bottom of the insert, just to the side of 4 of the 8 fuel passages. Each temp plug was placed at 90 deg increments around the circumference of the insert. Figure 34 shows the location of some of the temp plugs in the insert. The temp plugs near the top of the insert will register lower temperatures than the temp plugs at the bottom of the insert.

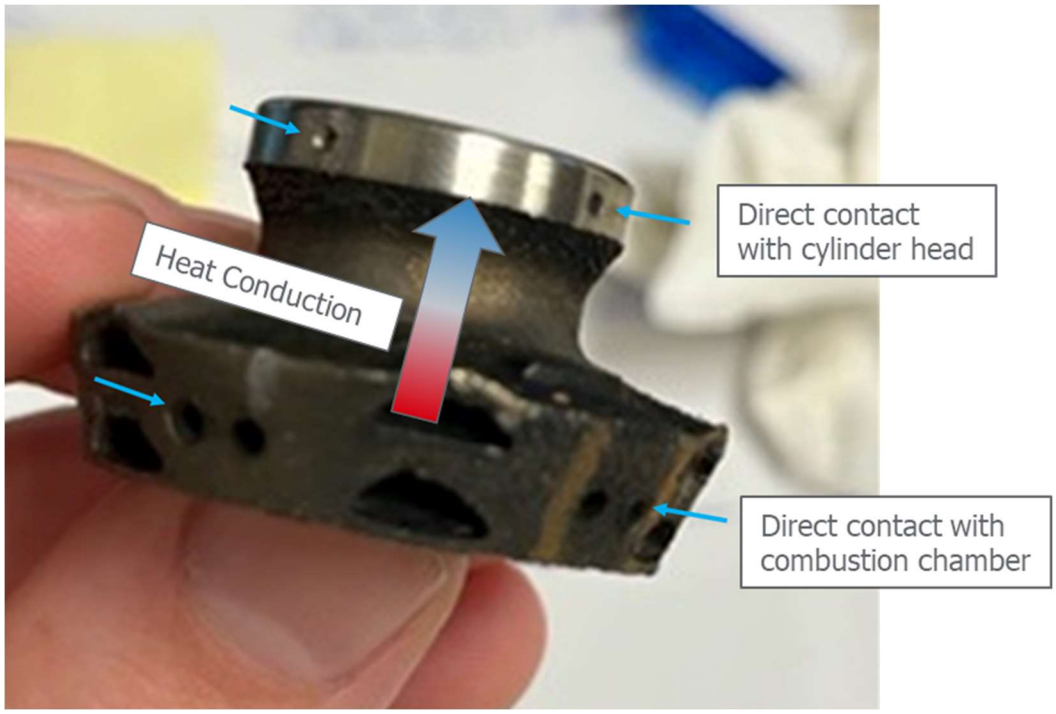

Figure 34: image of the CS insert with locations of Temp plugs.

The engine was run at Mode 10 (full load, rated speed) for several hours and the plugs were subsequently processed. The resulting temperatures are shown in Figure 35. The temperature measurements for the temp plugs at the top of the insert, in contact with the cylinder head, are labeled in blue (289-301° C). The measurements of the bottom of the insert (in direct contact with the combustion chamber) are detailed in red (446-514° C). Note that two of the temp plugs from the top of the insert were damaged and did not provide a reading.

The general trends of the data are in line with expectations. The temperatures near the cylinder head are cooler than the temperatures near the bottom of the insert because the top of the insert is in direct contact with the water-cooled cylinder head while the bottom of the insert is in direct contact with the hot combustion gases. Additionally, the bottom of the insert shows higher temperatures in the direction of the exhaust valves, which is also consistent with expectations. As cool air is drawn into the combustion chamber from the intake valves, it will cool the insert, but it will more directly cool the portion of the insert on the intake valve side of the cylinder head.

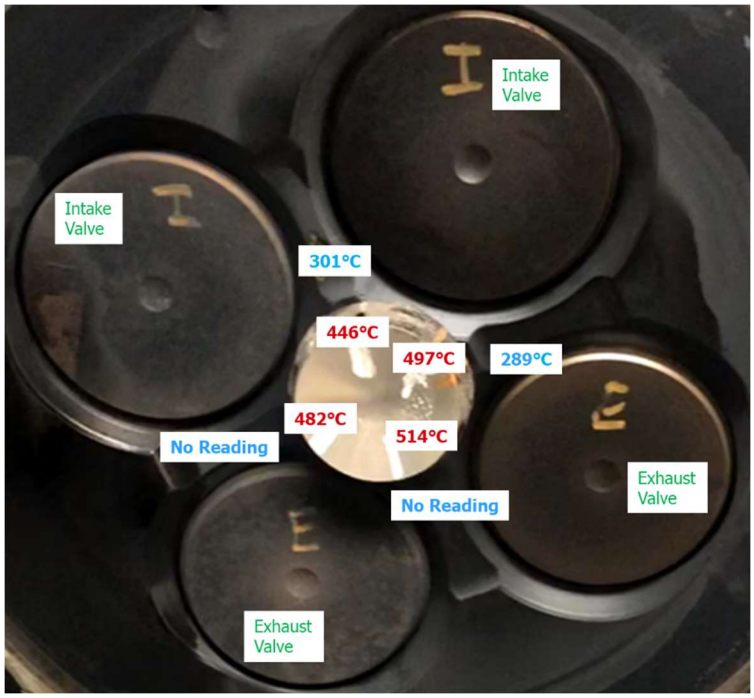

Figure 35: Temp plug results from CS testing.

The temperature measurements are lower than was estimated in the original analysis at the beginning of the project. Originally, the temperatures in the lower regions of the insert were calculated to be on the order of 800°C but these measurements suggest that the insert was reaching only about 500°C in this region. This lower temperature is promising because less thermal distortion will occur and fewer problems associated with misalignment or thermal stresses will be expected.

3. Geometry variations

A new series of inserts was designed and manufactured using the learnings from previous tests, and further evaluating the hydro-erosion methodology. Initial tests of the inserts from this batch generally showed poor performance and some testing was devoted to exploring the variants to better understand the reason for the poor performance. The hardware variants had geometric parameters similar to the inserts from Figure 33, but their performance was significantly worse. Possible causes of the performance shift could be related to repeatability/alignment, small changes that were made in the distance between the injector and fuel passage, changes that were made to the air passage geometry or changes in the hydro-erosion process. In this section, we evaluate which of these might be the cause of the performance shift.

Several sets of experiments were performed, evaluating different hardware geometries and the results of those tests are summarized below. Figure 36 shows the PM ratio for several sets of tests, normalized by the baseline non-CS configuration. A ratio of unity means that the configuration had the same average PM emissions as the baseline and a ratio of less than unity means that the configuration had lower PM emissions compared to the baseline. Each bar represents the average of 4 operating conditions: Mode 3 and Mode 8 with and without EGR and

the average was calculated with even weight for the 4 conditions. For configurations where multiple alignments were tested, the results of the best performing alignment is reported in this figure. In all cases, the injection timing was adjusted to run the same NOx emissions as the baseline.

The first two bars (Baseline and Best Insert) in the figure represent original test data for the baseline and hydro-eroded insert from the first batch of inserts produced with this method. The third bar (Best insert, repeat) shows the performance of that same insert, tested at a later date, around the same time as the testing of the new batch of hydro-eroded inserts.

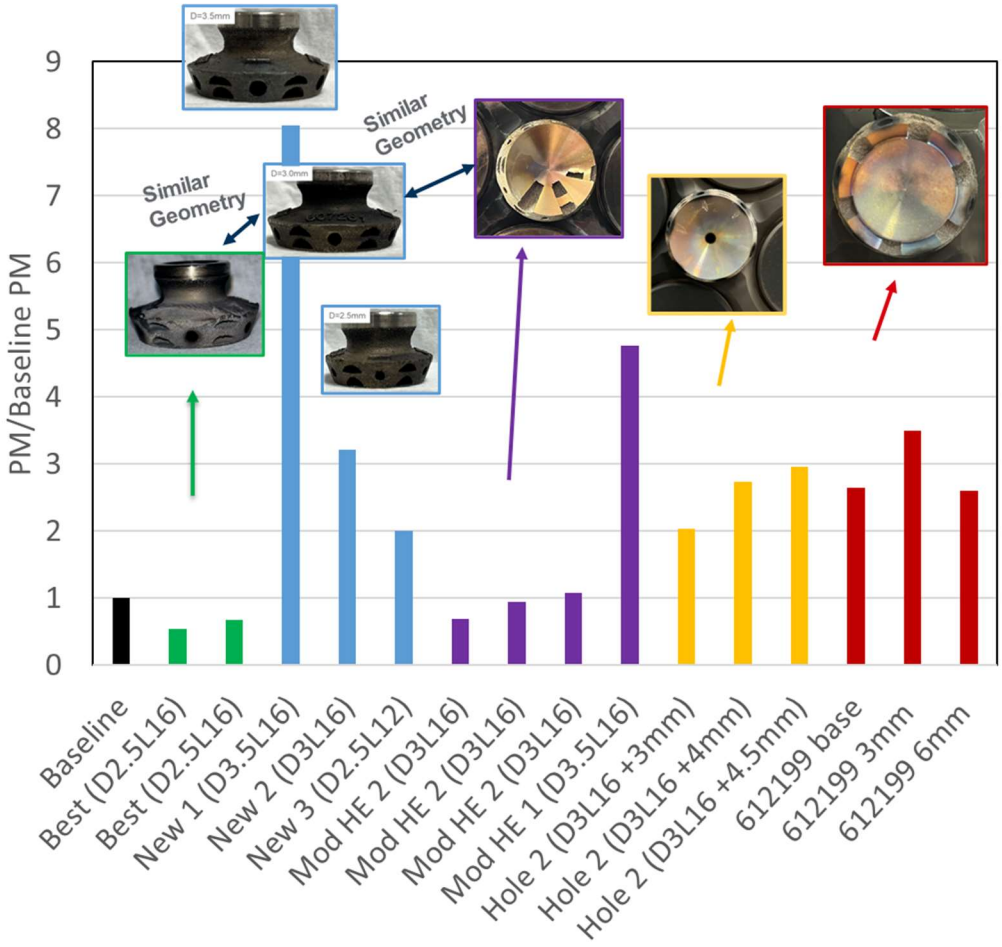

Figure 36: Comparison of Baseline non-Cooled Spray Tests to Various Cooled Spray configurations.

Hydro-eroded inserts similar in geometry to the first batch ('New Insert', D3.5, D3 & D2.5 in blue) showed poor performance, highlighting that some change in the insert design had a drastic effect on the insert performance. However, the good performance seen with the Best Insert under repeat conditions shows that the good performance is repeatable. The results show reasonable repeatability with the previous data and indicate that the performance degradation measured with the new inserts is likely not due to a repeatability issue.

In addition to validating repeatability, a series of alignment tests were performed to further test sensitivity to misalignment and the results are plotted in Figure 37. The best insert from the first batch of hydro-eroded inserts was used for this sensitivity study. The vertical misalignment

was changed by inserting and removing shims between the cylinder head and insert. Each time, the injector was realigned and the engine was run at the same 4 operating conditions. The plot reveals an interesting behavior where the PM decreases with negative misalignment (meaning the injector holes appear below the center of the fuel passages), but a peak appears around -0.13mm with PM reduction again at even lower misalignment levels. The reason for this peak is not clear. It may be caused by a worse than typical horizontal alignment although the procedure for alignment was similar for all cases and the alignment images don't suggest this to be the issue. It's also possible that the position of the injector nozzle compared to the insert is modifying the air-fuel interaction in some way that is causing an increase in PM emissions for that particular data set. More investigation is required to fully understand this behavior. However, it is clear from this plot that alignment variations of 0.2mm are not sufficient to explain the significant PM increase observed with the new inserts. Additionally, this data suggests that an alignment tolerance of ~0.05mm may be required to maintain good performance of the insert.

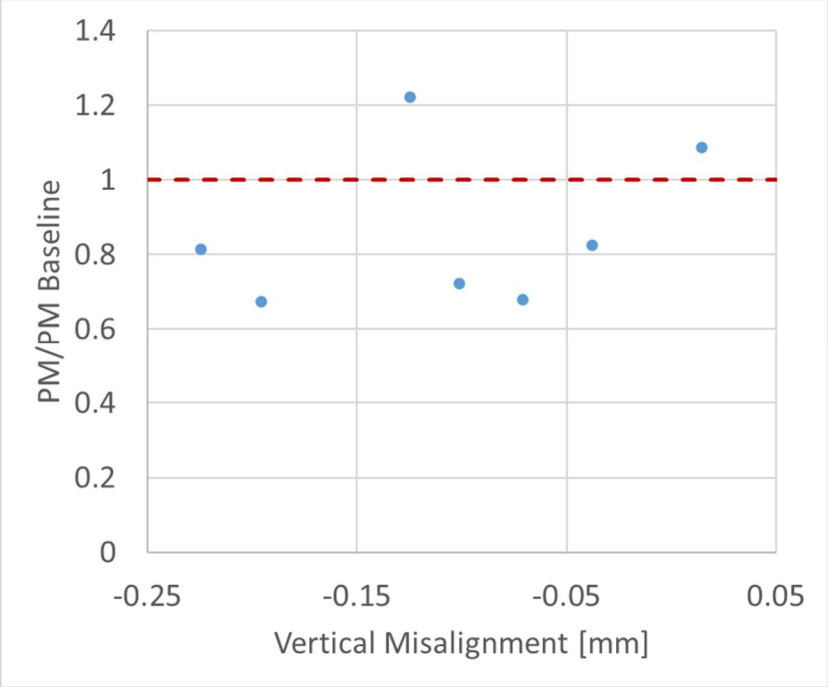

Figure 37: PM ratio results of a misalignment test.

The new batch of inserts utilized a hydro-erosion process to smooth out the printed fuel passages and create a rounded edge on the fuel passage inlet. However, that process was modified from the previous settings in an attempt to define a standard process of hydro-erosion that would polish the fuel passages without removing too much material. This resulted in changes to the hydro-erosion settings compared to those used for the 'Best Insert'.

When the insert geometries were printed, multiple copies of each were made so spare parts that had not experienced the hydro-erosion process were available. Two of these were used to re-run the hydro-erosion process with settings that more closely matched those of the best insert and those inserts with the modified hydro-erosion process were also tested on the engine (Figure 36, Mod HE D3 and D3.5). An interesting result is that the Mod HE D3 showed significant improvement in PM while the Mod HE D3.5 still showed high PM emissions.

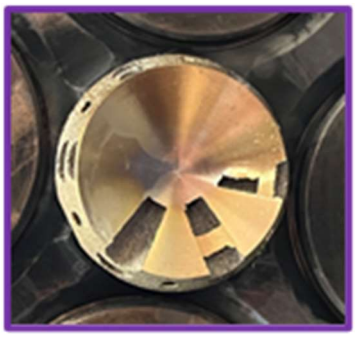

Figure 38: Image of Mod HE D3 insert after engine tests were completed.

When the Mod HE D3 insert was removed from the engine, it was found that some of the air passages had been damaged (Figure 38). This is the result of a printing error that caused thin walls in the bottom region of this insert. After being thermally stressed, some of the thin walls broke away inside the engine and opened up the air passages. Repeat studies were performed with this insert after the damage was observed and showed low PM, suggesting that the inadvertently modified air passages may have improved the PM emissions for this insert or at least they did not negatively impact the PM emissions.

The results from the modified HE inserts suggested that small changes to air passage design may be responsible for the poorer performance of this batch of inserts. Since the insert with the opened-up lower air passages showed good performance, it was decided that increasing the air flow area on the lower side of the insert might improve performance. To test this, a small hole was drilled in the bottom center of one of the inserts. The initial hole diameter was 3mm, and it was tested again with a 4 and 4.5 mm hole to see the effect (Figure 36, ‘Center Hole’ 3mm, 4mm and 4.5mm in yellow). The base geometry for this insert was the same as that showing the damaged lower air passages, however this insert did not show the same PM benefit. The trend with increasing center hole size suggests that maybe a smaller center hole could have provided more PM benefit, but it’s not clear if any center hole would have improved PM relative to the baseline.

A second modification was attempted where the lower air passages were cut away starting from the outside edge to more closely reflect the geometry change from the damaged insert. The base insert geometry was similar to that of the previous two iterations, but there were some small differences in the air passage geometry. A baseline test was first performed on the insert and then it was removed and the lower portion of the insert was machined from the outer 3mm of the insert and it was tested again. After this, another 3mm was removed and it was tested once again (‘New Insert’, 3mm/ ‘Mod Air Passage’, 3mm and 6 mm in red). The results show that the modifications did not have a significant beneficial impact on the PM emissions for the insert.

This study investigated several factors to determine the cause of the increased PM with the new inserts compared to the previous insert design. Specifically, repeatability, misalignment, hydro-erosion process and air passage design were all investigated. No clear cause was identified, but the results suggest that repeatability and misalignment are likely not the cause. Rather, we suspect that the cause may be related to the air passage design and the hydro-erosion process that was used.

4. Chamfered vs non-chamfered

Additional inserts were created where the fuel passages were drilled instead of printed. Some tests were performed to characterize the benefit of chamfering the fuel passage inlet of a drilled fuel passage. This investigation was motivated by previous work with DFI showing that rounding the duct inlet had a beneficial impact on performance[5]. When the fuel passages were printed and hydro-eroded, the inlet of the fuel passage was naturally rounded due to the nature of the hydro-erosion process, but when the fuel passages were drilled, no rounding existed and in many cases, a small amount of material protruded from the fuel passage inlet, as can be seen in Figure 39. Note that in these photos, the before and after pictures are from different inserts, but they illustrate the difference in the shape of the fuel passages with the chamfering process. A spherical grinding ball (3mm diameter) and high-speed rotary tool were used to grind material away and create the chamfer.

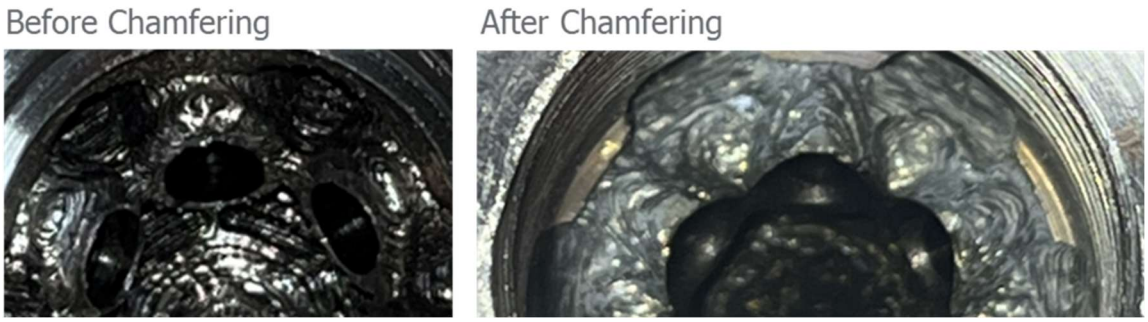

Figure 39: Image of fuel passage inlets before chamfering and after chamfering.

A study was performed on one insert to investigate the sensitivity of engine performance to the amount of chamfering on the fuel passage inlet. To quantify the amount of chamfering, the grinding tool was placed against the fuel passage inlet with the rotary tool turned off and a probe was inserted from the outside of the fuel passage until it contacted the grinding tool on the inside. The insertion depth of the probe was then measured. After material was incrementally ground away with the rotary tool, the insertion depth was remeasured to calculate the amount of material removed. The measurement was performed on each of the fuel passage holes and an average was used in the calculations and plots below.

Three chamfer depths were tested with the alignment kept as close as possible across the tests. The insert was first tested with no chamfering (0mm chamfer depth) and subsequently 0.6 and 1.2mm of material was ground away. The FSN is plotted versus the chamfer depth in Figure 40. For 3 of the 4 conditions, the FSN is reduced 50-75% as the chamfer depth is increased. However, at the Mode 8 non-EGR condition, the FSN increases by a factor of 2 for that same chamfering.

There are several possible reasons that chamfering is improving performance at some conditions and not at others. It is expected that the chamfering improves the ingestion of air and fuel into the fuel passages. However, it may be that at the highest load condition without EGR, there is sufficient space near the injector to allow combustion inside the fuel passage, thereby leading to increased FSN for that condition. Alternatively, the chamfering may increase the penetration of the fuel plume into the cylinder, leading to impingement at some conditions.

These results are consistent with what has been observed with other inserts where chamfering was employed. Chamfering improved performance at some operating conditions, but at other

operating conditions it was detrimental. Overall, it appears to benefit the FSN and soot emissions. Additional results can be found in [6].

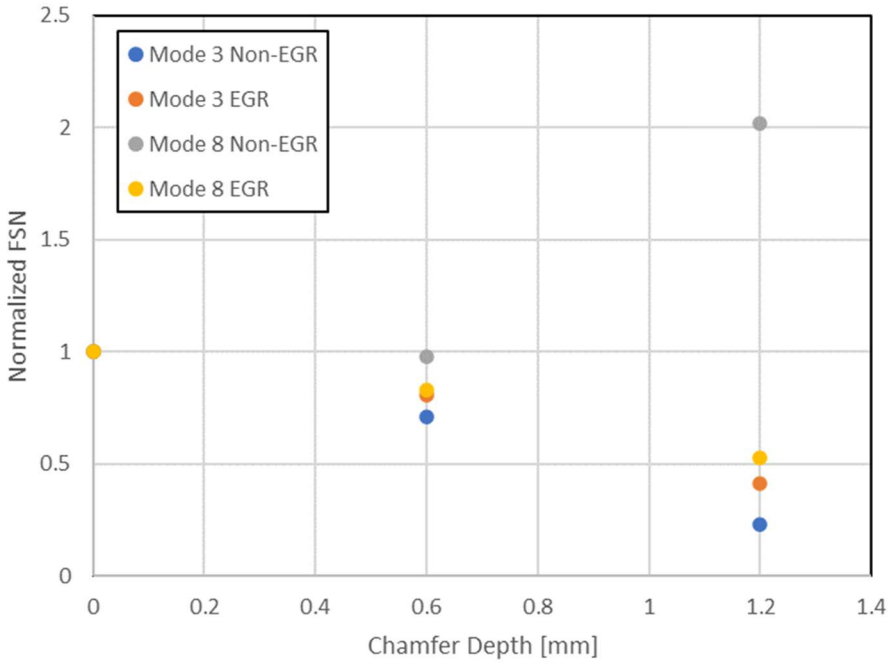

Figure 40: FSN versus chamfer depth.

5. Fuel passage diameter effects

A series of tests was performed to investigate the sensitivity of the FSN to fuel passage diameter in a CS insert. The inserts used for this study all used the same nominal geometry with a distance from the injector nozzle to the fuel passage inlet of approximately 3mm and a fuel passage length of approximately 16mm. However, the fuel passage diameters were varied from 2.2 to 2.8mm. A chamfer depth of approximately 1 to 1.2mm was used in all cases. Multiple vertical alignments were tested from -0.15mm (the injector nozzle is below the center of the fuel passage) to +0.2mm (the injector nozzle is 0.2mm above the center of the fuel passage).

The inserts were tested at multiple operating conditions and detailed results of those tests can be found in [6]. Summary results in Figure 41 show the minimum PM ratio versus the fuel passage diameter for 4 operating conditions. Note that the minimum PM ratio represents the lowest PM ratio for the insert with that fuel passage diameter across all the alignments investigated.

The alignment that provided the lowest PM ratio for the Mode 8 EGR condition may not be the same alignment that provided the lowest PM ratio for the Mode 3 conditions or the Mode 8 non-EGR condition. Nevertheless, the plot illustrates that at larger fuel passage diameters, the CS inserts generally are less effective, but at smaller fuel passage diameters, most of the CS inserts provide improved PM. The exception is the Mode 8 non-EGR condition which shows the lowest PM ratio with larger fuel passage diameters.

There are some important observations from these results. First, the data suggest that for this engine and nominal CS geometry, the best performing insert uses a fuel passage of ~2.4mm in diameter. Prior DFI results showed that for much smaller engines with much smaller fuel injector orifices, the duct diameter should also be on the order of 2-3mm. This suggests that the optimal fuel passage diameter in CS inserts and DFI modules may not be sensitive to engine size or fuel injector orifice size.

Another important observation is that the Mode 8 non-EGR condition shows increased FSN with small fuel passage diameter and lower PM with larger fuel passage diameter. While the Mode 8 EGR and the Mode 3 conditions generally show lower PM with lower fuel passage diameters. It is possible that the spray cone angle is changing with operating conditions (boost pressure and injection pressure vary across the 4 operating modes) and that may impact how much fuel is captured by the fuel passage. If the spray cone angle is wide, some of the fuel may impinge on the fuel passage inlet. That could explain why the operation at one condition is poor for smaller diameters and improves for larger diameters. It's also known that the CS inserts restrict the amount of air that is entrained with the fuel spray, causing the fuel spray to travel faster and penetrate further into the combustion chamber. This increased penetration may be playing a role in the performance differences observed for the smaller diameters.

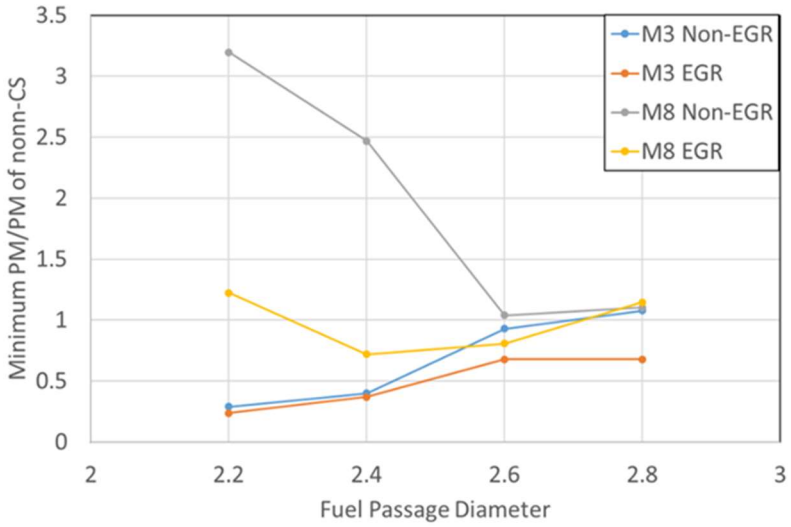

Figure 41: Minimum PM Ratio versus fuel passage diameter.

7. Air-Fuel Ratio Sensitivity

In some studies it was observed that conditions operating at higher AFR experienced greater PM reduction from CS than conditions with low AFR. An extensive study focused on testing the AFR sensitivity of a CS module. Low-, medium- and high- MAP settings were selected for each operating mode to represent a range of AFR conditions at each mode. A different set of MAP values was selected based on the operating mode and whether EGR was used. The engine was tested with and without CS at each of the MAP levels with and without EGR to characterize how

the effectiveness of the CS inserts changes with AFR. The MAP levels were selected to provide approximately 10% variations in air-fuel ratio.

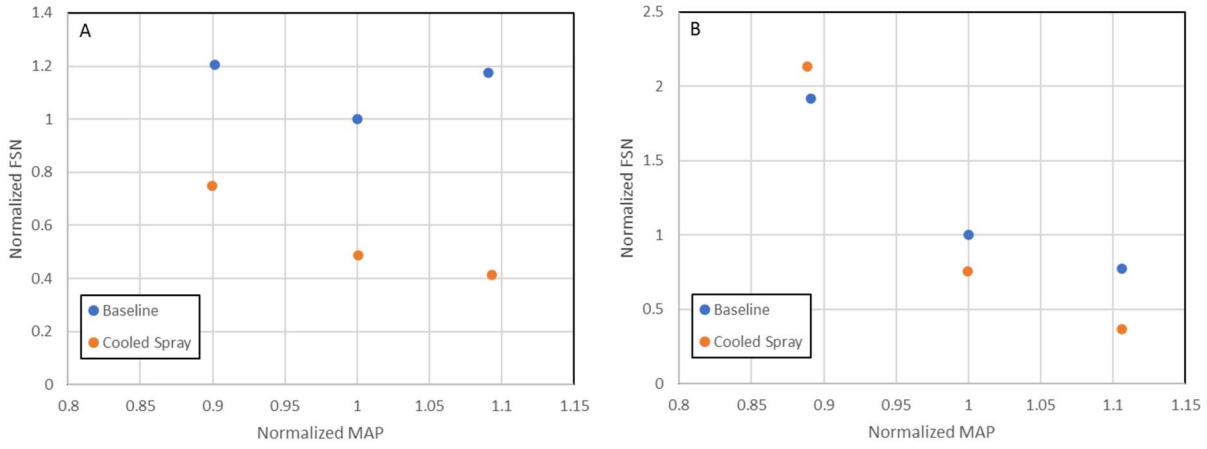

Figure 42: FSN versus MAP for Mode 10 operation. A-non EGR operation, B-EGR operation.

Sample results for Mode 10 operation are shown in Figure 42. The non-EGR tests were run at the same NOx level except at the highest boost pressure condition where the NOx was reduced approximately 10% to satisfy peak cylinder pressure constraints. Thus, as the MAP was increased, the FSN decreased, except for the highest MAP case without CS where FSN increased. For CS operation in the non-EGR condition, FSN decreased with increasing MAP even with the later injection timing and lower NOx condition of the highest MAP setting. One important detail to note is that the percentage decrease of FSN is greatest for the high MAP and lowest for the low MAP case. Thus, this data supports early observations that this CS insert reduces FSN (and thus PM) more effectively at higher AFR.

For EGR operation, all six points plotted in Figure 42B were recorded at the same nominal NOx emissions. As the MAP increases for both the baseline and CS operation, the FSN decreases. This is consistent with expectations for typical diesel engines. For this condition, at the lowest MAP condition, the baseline condition had lower FSN than the CS configuration, but at the higher MAP levels, the CS configuration reduced the FSN below that of the baseline non-CS configuration.

Similar tests were performed for all the operating modes with the exception of the idle condition and a duty cycle performance value was calculated for the high-, medium- and low-MAP sets of conditions. Figure 43 summarizes the change in duty-cycle performance going from non-CS baseline to CS operation for the three different sets of air-handling conditions. The plot shows that SFC increases for CS operation. For non-EGR operation, it increases by 2.5 to 3.5%. For EGR operation, it increases around 1.5 to 2%. It is also notable that the SFC degradation is not as severe for EGR operation at the higher AFR while for non-EGR operation, the SFC degradation is lowest at the low AFR condition.

The NOx variation for all conditions was very small because the tests were intentionally performed at constant NOx emissions. The PM emissions respond to the AFR differently between EGR and non-EGR operation. For non-EGR operation, the PM reduction of CS is on the order of 50% and very little sensitivity is observed across the different MAP settings. For EGR operation, the PM reduction of CS at the high MAP condition is approximately 50% while

at the lowest MAP setting, the PM increases by 50%. Thus, the EGR condition shows a strong sensitivity to MAP and AFR.

Hydrocarbon and CO emissions are increased with CS. These emissions are insensitive to MAP for the non-EGR condition, but there is some improvement relative to the baseline for the EGR condition.

Figure 44 plots the change in PM emissions for different operating conditions with EGR. Some operating conditions show strong sensitivity to the MAP. For example, Mode 10 and Mode 2 show good PM reduction at the high MAP condition, but show PM increases at the low MAP case. Other conditions like Mode 12 show less sensitivity to the MAP and AFR, but nearly all operating conditions show that the CS insert is less effective at low AFR than high AFR.

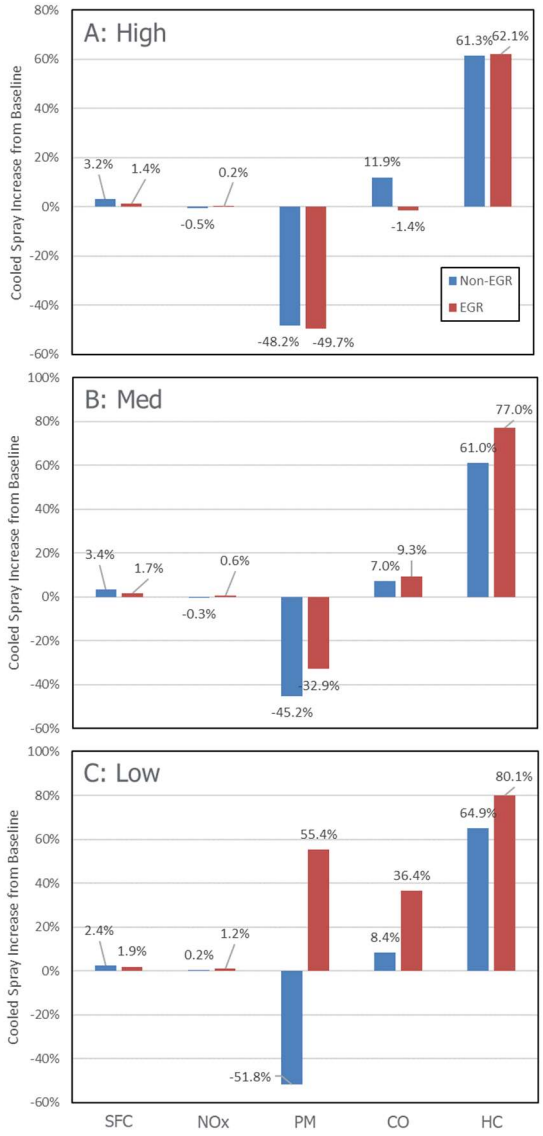

Figure 43: Duty cycle change in performance from baseline non-CS to CS operation at three different sets of air-handling conditions.

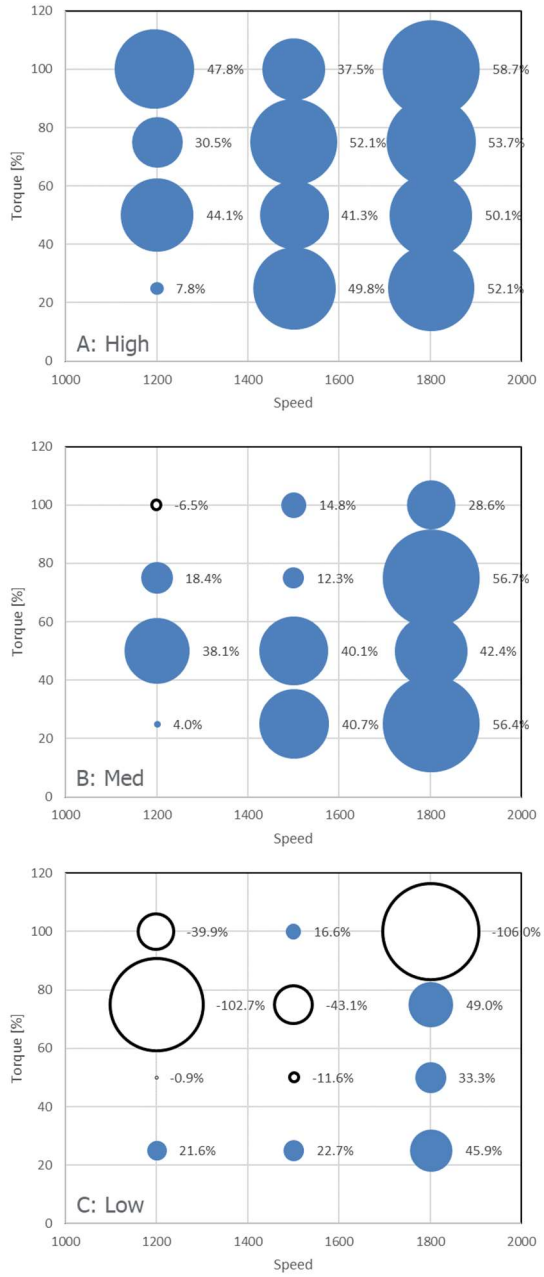

Figure 44: PM Reduction for CS versus non-CS baseline at different operating conditions with A-High, B-Medium and C-Low MAP settings for the EGR condition.

4. Final Performance Summary for Cooled Spray

The performance of CS technology has been evaluated over a large range of operating conditions with many CS designs. This section summarizes the best performance observed with CS. Figure 45 summarizes the best measured performance of CS relative to the equivalent baseline condition. These are duty cycle calculations based on the 13-mode SET and include idle operation. The non-EGR results show a 54% PM reduction over the duty cycle. One operating condition showed a PM reduction of over 80%, but most of the conditions did not show that level

of performance benefit. One interesting observation is that this non-EGR data was recorded approximately halfway through the project and showed a much smaller impact on fuel consumption than the more recent non-EGR data. It is possible that the performance of the engine has shifted or the most recent testing developed a defect with the cylinder head that was used for CS testing, but the true cause of this is not known.

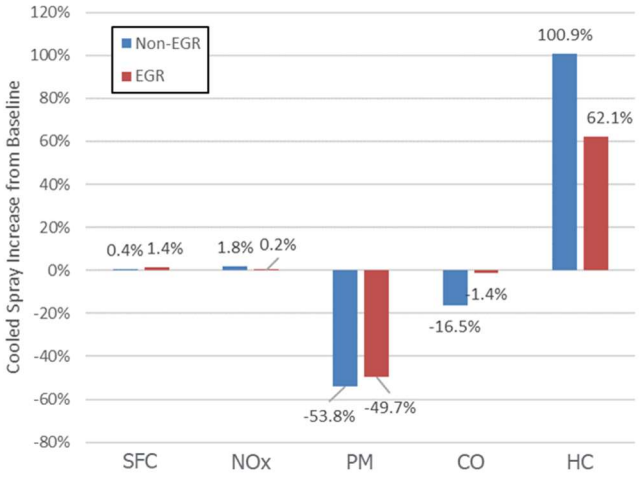

Figure 45: Summary of best performance data for CS operation. The reported summary data were obtained using an injector with a 0.29mm nozzle diameter.

The best EGR data set was taken from the high-MAP test results from the AFR variation study. Note that the high MAP tests were performed with CS and non-CS baseline at the same higher levels of MAP (~10% higher than the nominal settings) so the 50% improvement in PM from the CS configuration tested here is based on equivalent MAP values between the CS and non-CS tests. There was an increase in HC emissions for EGR and non-EGR operation, and the increase in HC emissions should be monitored as this technology is developed.

6. Project Summary

Cooled Spray and Ducted Fuel Injection were investigated on single-cylinder research engines to investigate the scaling relationships for these technologies and to characterize the performance of Cooled Spray technology over a broad operating range. The results presented here suggest that for injectors with large orifice diameters (0.29-0.31mm) the optimal fuel passage diameter for CS and DFI hardware is approximately 2.5mm, but it isn't clear if the smallest diameter fuel passages performed poorly because they are not optimal or because they are more challenging to align. Smaller diameters may be effective if the required alignment accuracy can be achieved and future work should investigate this possibility. Larger diameters resulted in higher particulate emissions. Interestingly, previous published data has shown that for fuel injector orifices in the range of 0.1-0.14mm, DFI duct diameters of ~2-3mm performed well. This suggests that the optimal fuel passage diameter may not be sensitive to the injector diameter and no scaling may be required.

It was shown that the performance of the insert is sensitive to misalignment with some inserts requiring the alignment be within ~0.05mm of optimal to provide reasonable PM reduction. Other data not presented here but summarized in a submitted conference paper [6] showed that some geometries are more tolerant to misalignment, but still requiring alignment to be within

~0.1mm for best performance. It was also shown that for CS inserts, rounding or chamfering of the fuel passage inlet is important for best performance. This is consistent with previous DFI results that are reported in the literature.

The test data also show that the CS inserts used here were more effective at reducing PM emissions for higher AFR conditions. A focused study on AFR sensitivity showed that when the AFR was increased for both non-CS baseline and CS conditions, the CS configuration showed even more relative PM reduction than at the original AFR conditions. This sensitivity was not observed at all conditions, but was consistent for many of the operating conditions.

Final summarized test results show that the duty-cycle PM emissions were reduced by approximately 50% for both EGR and non-EGR duty cycles using CS technology with PM reductions as high as 80% at some operating conditions. Fuel consumption increased between 0.4 and 1.4% for the CS tests on the duty cycle calculations. It is hypothesized that the increase in fuel consumption may be caused by heat losses or unidentified damage to the cylinder head. Additional design optimization may improve the fuel consumption for this engine.

References

[1] EPA, 2016, “Greenhouse Gas Emissions and Fuel Efficiency Standards for Medium- and Heavy-Duty Engines and Vehicles—Phase 2, U.S. Environmental Protection Agency (EPA),” Final Rule, Federal Register, 81(206), pp. 73478–74274.

[2] Buurman, N., Nyrenstedt, G., and Mueller, C., "Ducted Fuel Injection Provides Consistently Lower Soot Emissions in Sweep to Full-Load Conditions," Engines 17(1):3-16, 2024, https://doi.org/10.4271/03-17-01-0001.

[3] Klingbeil, A, Heher, B, Flores, M, Triana Padilla, A, Lavertu, T, Tinar, T, & Ellis, S. "Cooled Spray Technology for Particulate Reduction in a Heavy-Duty Engine." *Proceedings of the ASME 2022 ICE Forward Conference*. *ASME 2022 ICE Forward Conference*. Indianapolis, Indiana, USA. October 16–19, 2022. V001T03A009. ASME. https://doi.org/10.1115/ICEF2022-90604

[4] Klingbeil, A, Tinar, T, Ellis, S. "Cooled Spray Technology for Particulate Reduction in a Heavy-Duty Engine." ASME. *J. Eng. Gas Turbines Power*. In Press.

[5] Gehmlich, R. K., Mueller, C. J., Ruth, D. J., Nilsen, C. W., Skeen, S. A., and Manin, J., 2018, “Using Ducted Fuel Injection to Attenuate or Prevent Soot Formation in Mixing-Controlled Combustion Strategies for Engine Applications,” Appl. Energy, 226, pp. 1169–1186

[6] Klingbeil, A, Tinar, T. "Investigation of Fuel Passage Geometry on Performance of Cooled Spray Inserts for Particulate Reduction in a Heavy-Duty Engine." *Submitted to ASME 2024 ICEF*